Mitochondrial glycolysis in a major lineage of eukaryotes

Carolina Río Bártulos[1,8], Matthew B. Rogers[2$], Tom A. Williams[3], Eleni Gentekaki[4&], Henner Brinkmann[5%], Rüdiger Cerff[1], Marie-Françoise Liaud[1], Adrian B. Hehl[6], Nigel R. Yarlett[7], Ansgar Gruber[8§], Peter G. Kroth[8]*, Mark van der Giezen[2]*

[1]Institute of Genetics, University of Braunschweig, 38106 Braunschweig, Germany.

[2]Biosciences, University of Exeter, Stocker Road, Exeter EX4 4QD, United Kingdom.

[3] School of Biological Sciences, University of Bristol, Bristol BS8 1TH, United Kingdom.

[4]Department of Biochemistry and Molecular Biology, Dalhousie University, Halifax B3H 1X5, Canada.

[5]Département de Biochimie, Université de Montréal C.P. 6128, Montréal, Quebec, Canada.

[6]Institute of Parasitology, University of Zürich, Switzerland.

[7]Department of Chemistry and Physical Sciences, Pace University, New York, NY 10038, USA.

[8]Fachbereich Biologie, Universität Konstanz, 78457 Konstanz, Germany.

*Correspondence to: peter.kroth@uni-konstanz.de, m.vandergiezen@exeter.ac.uk

[$]Current address: Rangos Research Center, University of Pittsburgh, Children's Hospital, Pittsburgh, PA 15224, U.S.A.

[&]Current address: School of Science and Human Gut Microbiome for Health Research Unit, Mae Fah Luang University, Chiang Rai 57100, Thailand.

[%]Current address: Leibniz-Institut DSMZ - Deutsche Sammlung von Mikroorganismen und Zellkulturen GmbH, Inhoffenstraße 7 B, D-38124 Braunschweig, Germany.

[§]Current address: Institute of Parasitology, Biology Centre, Czech Academy of Sciences, Branišovská 1160/31, 37005 České Budějovice, Czech Republic.

Abstract

The establishment of the mitochondrion is seen as a transformational step in the origin of eukaryotes. With the mitochondrion came bioenergetic freedom to explore novel evolutionary space leading to the eukaryotic radiation known today. The tight integration of the bacterial endosymbiont with its archaeal host was accompanied by a massive endosymbiotic gene transfer resulting in a small mitochondrial genome which is just a ghost of the original incoming bacterial genome. This endosymbiotic gene transfer resulted in the loss of many genes, both from the bacterial symbiont as well the archaeal host. Loss of genes encoding redundant functions resulted in a replacement of the bulk of the host's metabolism for those originating from the endosymbiont. Glycolysis is one such metabolic pathway in which the original archaeal enzymes have been replaced by the bacterial enzymes from the endosymbiont. Glycolysis is a major catabolic pathway that provides cellular energy from the breakdown of glucose. The glycolytic pathway of eukaryotes appears to be bacterial in origin, and in well-studied model eukaryotes it takes place in the cytosol. In contrast, here we demonstrate that the latter stages of glycolysis take place in the mitochondria of stramenopiles, a diverse and ecologically important lineage of eukaryotes. Although our work is based on a limited sample of stramenopiles, it leaves open the possibility that the mitochondrial targeting of glycolytic enzymes in stramenopiles might represent the ancestral state for eukaryotes.

Keywords

Glycolysis, mitochondria, organelle, stramenopile, evolution, compartmentalisation.

Introduction

Mitochondria provide the bulk of cellular ATP for eukaryotes via oxidative phosphorylation, also known as cellular respiration (Müller, et al. 2012). In addition, mitochondria are essential for the production of iron-sulfur clusters (Lill, et al. 1999) and play roles in heme synthesis, in fatty acid and in amino acid metabolism (Scheffler 2008). For cellular respiration, pyruvate is produced in the cytosol via glycolysis and imported into the mitochondrion. The pyruvate is then decarboxylated by a mitochondrial pyruvate

dehydrogenase to acetyl-CoA. This acetyl-CoA enters the citric acid cycle, subsequently producing one GTP (or ATP) and precursors for several anabolic pathways. More importantly, the reduction of NAD^+ to NADH and the production of succinate power the respiratory electron transport chain and subsequently ATP synthesis by the proton gradient driven ATP synthase, which is responsible for the majority of cellular ATP synthesis.

Glycolysis, the pathway that produces the pyruvate, is a widespread metabolic pathway that converts the six-carbon sugar glucose via a series of ten reactions into the three-carbon sugar pyruvate. During this conversion, energy is stored (two ATP per glucose) and reducing equivalents are formed (two NADH per glucose). To keep the pathway going, NADH needs to be recycled to NAD^+, which can happen in a fermentative process, most commonly leading to the formation of lactic acid or ethanol in the cytosol, or by shuttling of the reducing equivalents to the mitochondrial respiratory electron transport chain, which leads to an increased ATP yield.

Glycolysis is present in all known eukaryotes, with the exception of some extremely reduced intracellular parasites (Keeling, et al. 2010; Wiredu Boakye, et al. 2017). Glycolysis is nearly universally present in the cytosol of most eukaryotes and also found in specialised microbodies known as glycosomes, originally found in trypanosomes (Opperdoes and Borst 1980), but more recently found to be perhaps a more general feature of all the euglenozoa (Morales, et al. 2016). Two glycolytic enzymes were also found to be targeted to peroxisomes in fungi due to post-transcriptional processes (Freitag, et al. 2012). An unusual TPI-GAPDH fusion protein was reported to localise to the mitochondrion of a stramenopile, the diatom *Phaeodactylum tricornutum* (Liaud, et al. 2000). In addition, bioinformatics studies (Kroth, et al. 2008; Nakayama, et al. 2012) have hinted at the possible mitochondrial location of several glycolytic enzymes.

Stramenopiles are a large and extremely diverse eukaryotic group of organisms, including phototrophic members such as the multicellular kelps (brown algae) and unicellular microalgae including diatoms. They also include non-phototrophic members such as oomycetes, plant pathogens with an enormous impact on agriculture (Jiang and Tyler 2012) and the human pathogen *Blastocystis* (Stensvold and van der Giezen 2018). The latter species has an anaerobic lifestyle and lacks many features commonly found in mitochondria (Gentekaki, et al. 2017; Müller, et al. 2012). The stramenopiles evolved by endosymbiotic uptake of a red alga but the question as to whether the non-photosynthetic members never possessed a plastid, or simply lost it, remains unclear (Baurain, et al. 2010; Derelle, et al. 2016; Petersen, et al. 2014). Members of the stramenopiles can be found in most ecosystems on earth: in marine and fresh water

environments, in soil, and as pathogens of humans, animal and plants. Despite their enormous variety in lifestyle a clear monophyly of this group is undisputed (Derelle, et al. 2016; Walker, et al. 2011).

Here, we report that the second half of glycolysis, the C3 part, is targeted to mitochondria in the stramenopiles. This exclusive feature of the stramenopiles might be a synapomorphy of this large group of eukaryotes. Mitochondrial glycolysis only covers the pay-off phase of glycolysis, in which the three carbon sugars are converted to pyruvate, leading to the release of energy and reducing equivalents in the form of ATP and NADH.

Material and Methods

Sources of cDNA and genomic DNA

DNA and cDNA from *Blastocystis* ST1 strain NandII, obtained from a symptomatic human (strain obtained from the American Type Culture Collection, ATCC 50177), was used in this study. Genomic and cDNA libraries of *Phaeodactylum tricornutum* (culture from SAG strain: 1090-1a, Göttingen) were constructed with the "Lambda ZAP II XR library Construction Kit" from Stratagene and the lambda vector EMBL3, respectively. *P. tricornutum* Bohlin (strain 646; University of Texas Culture Collection, Austin) RNA was isolated using TRIzol following manufactures protocol (Thermo Fisher, Germany) and cDNA synthesis was performed with the reverse Transcription system (A3500, Promega, Germany). An *Achlya bisexualis* cDNA library (Bhattacharya, et al. 1991) was kindly provided by D. Bhattacharya (Rutgers University). Screening of libraries, sequencing of positive clones and RACE analyses were performed as described (Liaud, et al. 1997). *Phytophthora infestans* RNA extracted from *P. infestans* mycelia with the RNAeasy Plant Kit from Quiagen and cDNA was synthesized with the Thermo-RT Kit (Display Systems, England). Sequences were also obtained from the EST/genome sequencing programmes from *Phaeodactylum tricornutum* (Maheswari, et al. 2005) and http://genome.jgi-psf.org/Phatr2/Phatr2.home.html (JGI)(Bowler, et al. 2008), from *Phytophthora infestans* (http://www.pfgd.org (Tripathy, et al. 2006)) and from *P. sojae* and *P. ramorum* (http://www.jgi.doe.gov (Tyler, et al. 2006)).

GFP constructs for the stable transformation of *Phaeodactylum tricornutum*

Standard cloning procedures were applied (Sambrook, et al. 1989). Polymerase chain reaction (PCR) was performed with a Master Cycler Gradient (Eppendorf) using Taq DNA Polymerase (Q BIOgene) according to

the manufacturer's instructions. cDNA from *Blastocystis* ST1 strain NandII (Bl), *Phaeodactylum tricornutum* (Pt), *Phytophthora infestans* (Pi) and *Achlya bisexualis* (Ab) was used as template for the PCR reactions. For *Saccharina latissima* (Sl) a cDNA clone (NCBI: ABU96661) was used as template. PCR products were cloned into TA-vector PCR 2.1 (Invitrogen) or blunt cloned into pBluescript II SK+ (Stratagene). The primers (Supplementary Table 1) allowed insertion of restriction enzyme recognition sites (*Eco*RI/*Nco*I or *Sma*I/*Nco*I) that were used to clone the presequences in frame to eGFP within pBluescript-GFP. The presequence-GFP fusions were cut out with appropriate restrictions enzymes (*Eco*RI/*Hin*dIII or *Sma*I/*Hin*dIII) and cloned into the *Phaeodactylum tricornutum* transformation vector pPha-T1 (Gruber, et al. 2007; Zaslavskaia, et al. 2000), either into the corresponding sites or, in case of *Sma*I, into the *Eco*RV site. For the constructs with Protein ID (Fig. 5) a slightly different cloning approach was used. PCR with a proof reading Polymerase (*Pfu* or Kapa Hifi) were used to amplify corresponding fragments from cDNA. The fragments were cloned blunt end in a modified pPha-T1 Vector. The vectors include an eGFP with a *Stu*I or *Ksp*AI restriction site, allowing a one-step cloning procedure, with subsequent screening for the correct orientation of the fragment at the N-terminus of eGFP. The *Blastocystis* presequences were produced by kinasing the primers using T4 polynucleotide kinase using manufacturer's procedures and subsequently annealing in a thermal cycler after which they were cloned into the diatom expression vector equipped with eGFP and the *Stu*I restriction site.

Cultivation and Transformation of *Phaeodactylum tricornutum*

Phaeodactylum tricornutum Bohlin (UTEX, strain 646) was grown at 22 °C under continuously light of 75 µE in artificial seawater (Tropic Marin) at a 0.5 concentration. Transformations were performed as described by Zaslavskaia *et al*. (Kroth 2007; Zaslavskaia, et al. 2000). For each transformation, tungsten particles M10 (0.7 µm median diameter) covered with 7-20 µg DNA were used to bombard cells with the Particle Delivery System PDS-1000 (Bio-Rad, HE-System) prepared with 650, 900, 1100 or 1350 psi rupture discs.

Microscopic analysis of transformed *Phaeodactylum tricornutum*

Reporter gene expression was visualized using confocal laser scanning microscopy (cLSM-510META, Carl Zeiss, Jena, Germany) using a Plan-Neofluar 40x/1.3 Oil DIC objective. The eGFP fusion proteins were

excited with an argon laser at 488 nm with 8-10% of laser capacity. Excited fluorophores were detected with a bandpass filter GFP (505-530 nm) using a photomultiplier. Chlorophyll *a* autofluorescence was simultaneously detected with a META-channel (644-719 nm). MitoTraker Orange CM-H_2TMRos (Molecular Probes) was applied for fluorescence staining of mitochondria. *P. tricornutum* cells were stained according to the protocol of the manufacturer. Cells were incubated with 100 nM dye solution, incubated for 30 minutes, washed and observed (images were recorded using the Multitracking mode with the following parameters for Wavelength T1 = 488 nm 10% and T2 = 543 nm 100% laser line, primary beam splitting mirrors UV/488/543/633 nm; emitted light was detected with the META-channel).

Protein production and antibody generation

Blastocystis TPI-GAPDH was amplified from cDNA using primers TPI-GAPDH pET F: aga aga *CAT ATG* TTC GTC GGT GGC AAT TGG AAG TGC AA and TPI-GAPDH pET R: tct tct *GGA TCC* TTA AGA GCG ATC CAC CTT CGC CA adding *Nde*I and *Bam*HI restriction sites, respectively, to facilitate cloning in gene expression vector pET14b (Novagen, Merck, Whatford, UK). The *Blastocystis* PGK was amplified from cDNA using PGK pET F: aga aga *CAT ATG* AAG CTG GGA GTT GCT GCC TAC G and PGK pET R: tct tct *CAT ATG* TCA CGC GTC CGT CAG AGC GGC CAC ACC C which added *Nde*I restriction sites for pET14b cloning. The mitochondrial targeting signals were not amplified as these would not be part of the mature processed protein. All constructs were confirmed by sequencing. The in-frame His-tag allowed for affinity chromatography purification of the recombinant protein. Recombinant *Blastocystis* TPI-GAPDH and PGK were used to immunise guinea pigs and rabbits, respectively, for polyclonal antibody generation at Eurogentec (Seraing, Belgium).

Culture conditions for *Blastocystis*

Blastocystis isolate B (originally designated *Blastocystis* sp. group VII (Noel, et al. 2005), now called ST7 (Stensvold, et al. 2007)) was used. The parasite was grown in 10 ml pre-reduced Iscove's modified Dulbecco's medium (IMDM) supplemented with 10% heat-inactivated horse serum. Cultures were incubated for 48 h in anaerobic jars using an Oxoid AneroGen pack at 37 ^{o}C. Two-day-old cultures were centrifuged at 1600 g for 10 min, washed once in a buffer consisting of 30 mM potassium phosphate, 74 mM NaCl, 0.6 mM $CaCl_2$ and 1.6 mM KCl, pH 7.4 and resuspended in a nitrogen gassed isotonic buffer

consisting of 200 mM sucrose (pH 7.2) containing 30 mM phosphate, 15 mM mercaptoethanol, 30 mM NaCl, 0.6 mM $CaCl_2$, and 0.6 mM KCl (pH 7.2).

Confocal microscopy of *Blastocystis*

Blastocystis trophozoites were treated with MitoTracker Red (Molecular Probes), washed, fixed in 10% formalin and incubated in ice cold acetone for 15 minutes and air-dried.

Slides with fixed parasites were rehydrated in phosphate buffered saline (PBS) for 30 minutes and blocked with 2% BSA in PBS for 1 hour at room temperature. All antibody incubations were performed at room temperature in 2% BSA in PBS, 0.1% triton X-100. Slides were washed 5 times in 0.2 % BSA in PBS, 0.01% triton X-100 between incubations to remove unbound antibodies.

Primary antibodies: Rabbit, anti-PGK; Guinea Pig, anti-TPI-GAPDH (Eurogentec, Seraing, Belgium) were used at a dilution of 1:500 and 1:300 in 2% BSA in PBS, 0.1% triton X-100, respectively.

Secondary antibodies: Alexa Fluor 488 conjugated Goat anti-Rabbit (Invitrogen, Eugene, OR, USA), Alexa Fluor 405 conjugated Goat anti-Rabbit (Invitrogen, Eugene, OR, USA), TRITC-conjugated Goat anti-Guinea Pig were used at 1:200 dilutions in 2% BSA in PBS, 0.1% triton X-100, each.

The DNA intercalating agent 4'-6-Diamidino-2-phenylindole (DAPI) for detection of nuclear and mitochondrial DNA was added to the final but one washing solution at a concentration of 1 $\mu g \cdot ml^{-1}$. The labeled samples were embedded in Dako Glycergel Mounting Medium (DAKO, Carpinteira, CA, USA) and stored at 4 °C.

Immunofluorescence analysis and image data collection was performed on a Leica SP2 AOBS confocal laser-scanning microscope (Leica Microsystems, Wetzlar, Germany) using a glycerol immersion objective lens (Leica, HCX PL APO CS 63x 1.3 Corr). Image z-stacks were collected with a pinhole setting of Airy 1 and twofold oversampling. Image stacks of optical sections were further processed using the Huygens deconvolution software package version 2.7 (Scientific Volume Imaging, Hilversum, NL). Three-dimensional reconstruction, volume and surface rendering, and quantification of signal overlap in the 3D volume model were generated with the Imaris software suite (Version 7.2.1, Bitplane, Zurich, Switzerland). The degree of signal overlap in the 3D volume model is depicted graphically as scatterplots. The intensity of two fluorescent signals in each voxel of the 3D model is measured and plotted. Voxels

with similar signal intensity for both signals appear in the area of the diagonal. All image stacks were corrected for spectral shift before rendering and signal colocalization analysis.

Subcellular fractionation of *Blastocystis*

Blastocystis cells were broken by mixing 2 volumes of the cell suspension with 3 volumes of 0.5 mm beads and broken by 3 one minute duration shakes at maximum speed on a bead breaker (VWR mini bead mill homogenizer, Atlanta, GA, USA) with one-minute pauses on ice. Cell-free extracts were subjected to increasing centrifugal force producing nuclear (N, 1,912 RCF_{av} for 5 min), mitochondria-like (ML, 6,723 RCF_{av} for 15 min), lysosomal (L, 26,892 RCF_{av} for 30 min) and cytosolic (S) fractions, respectively, using a using a Sorvall RC-2B centrifuge fitted with an SS-34 rotor.

Enzyme assays

Hexokinase was assayed by measuring the reduction of NAD^+ at 340 nm in a coupled reaction with *Leuconostoc mesenteroides* glucose-6-phophate dehydrogenase (3 EU), containing 38 mM Tris-HCl pH 7.6, 115 mM D-glucose, 10 mM $MgCl_2$, 0.5 mM ATP, 0.2 mM NAD^+, 0.05 mL of *Blastocystis* cell-free extract (0.08-0.12 mg) or fraction (N, 0.15-0.18 mg; ML, 0.12-0.17 mg; L, 0.08-0.11 mg; S, 0.09-0.05 mg), in a final volume of 1 mL at 25 ^oC.

Phosphoglucose isomerase was assayed by measuring contained g the reduction of $NADP^+$ at 340 nm in a coupled reaction with *Leuconostoc mesenteroides* glucose-6-phophate dehydrogenase (2 EU), containing 38 mM Tris-HCl pH 7.6, 3.3 mM D-fructose-6-phosphate, 0.66 mM β-$NADP^+$, 3.3 mM $MgCl_2$, 0.05 mL of *Blastocystis* cell-free extract or fraction in a final volume of 3 mL at 25 ^oC.

Phosphofructokinase was assayed using the standard coupled assay containing 38 mM Tris-HCl pH 7.6, 5 mM dithiothreitol, 5 mM $MgCl_2$, 0.28 mM NADH, 0.1 mM ATP, 0.1 mM AMP, 0.8 mM fructose-6-ohosphate, 0.4 mM $(NH_4)_2SO_4$, 0.05 EU each of rabbit muscle aldolase, rabbit muscle glycerophosphate dehydrogenase, and rabbit muscle triosephosphate isomerase, 0.05 mL of *Blastocystis* cell-free extract or fraction in a final volume of 3 mL at 25 ^oC.

Aldolase was assayed using a modification of the hydrazine method in which 3-phosphoglyceraldehyde reacts with hydrazine to form a hydrazone which absorbs at 240 nm; the assay contained 12 mM fructose-

1,6-bisphosphate, pH 7.6, 0.1 mM EDTA, 3.5 mM hydrazine sulfate and 0.05 mL of *Blastocystis* cell-free extract or fraction in a final volume of 3 mL at 25 ^{o}C.

Triosephosphate isomerase was assayed by measuring the oxidation of NADH using a linked reaction with glycerol-3-phosphate dehydrogenase; 220 mM triethanolamine pH 7.6, 0.20 mM DL-glyceraldehyde-3-phosphate, 0.27 mM NADH, 1.7 EU glycerol-3-phosphate dehydrogenase, and 0.05 mL of *Blastocystis* cell-free extract or fraction in a final volume of 3 mL at 25 ^{o}C.

Glyceraldehyde-3-phosphate dehydrogenase was assayed by measuring the initial reduction of NAD^{+} at 340 nm; the assay contained 13 mM sodium pyrophosphate pH 8.0, 26 mM sodium arsenate, 0.25 mM NAD, 3.3 mM dithiothreitol, and 0.05 mL of *Blastocystis* cell-free extract or fraction in a final volume of 3 mL at 25 ^{o}C.

Phosphoglycerate kinase was assayed by measuring the 3-phosphoglycerate dependent oxidation of NADH at 340 nm; the assay contained 40 mM Tris-HCl pH 8.0, 0.5 mM $MgCl_2$, 0.26 mM NADH, 0.1 mM ATP, 2 EU *S. cerevisiae* glyceraldehydephosphate dehydrogenase, and 0.05 mL of *B. hominis* cell free extract or fraction in a final volume of 3 mL at 25 ^{o}C.

Phosphoglycerate mutase was measured using the standard coupled assay and measuring the decrease in absorbance at 340 nm; the assay contained 76 mM triethanolamine pH 8.0, 7 mM D(-) 3- phosphoglyceric acid, 0.7 mM ADP, 1.4 mM 2,3-diphosphoglyceric acid, 0.16 mM NADH, 2.6 mM $MgSO_4$, 100 mM KCl, 5 EU pyruvate kinase/8 EU lactate dehydrogenase from rabbit muscle, 5 EU rabbit muscle enolase, and 0.05 mL of *Blastocystis* cell-free extract or fraction in a final volume of 3 mL at 25 ^{o}C.

Enolase was determined using the standard coupled assay and measuring the decrease in absorbance at 340 nm; the assay contained 80 mM triethanolamine pH 8.0, 1.8 mM D(+) 2-phospholycerate, 0.1 mM NADH, 25 mM $MgSO_4$, 100 mM KCl, 1.3 mM ADP, 5 EU pyruvate kinase/8 EU lactate dehydrogenase from rabbit muscle, and 0.05 mL of *Blastocystis* cell-free extract or fraction in a final volume of 3 mL at 25^{o}C.

Pyruvate kinase was determined by measuring the oxidation of NADH at 340 nm using the following mixture, 45 mM imidazole-HCl pH 8.0, 1.5 mM ADP, 0.2 mM NADH, 1.5 mM phosphoenolpyruvate, 5 EU rabbit muscle lactate dehydrogenase, and 0.05 mL of *Blastocystis* cell-free extract or fraction in a final volume of 3 mL at 25 ^{o}C.

Pyruvate phosphate dikinase was assayed spectrophotometrically by measuring the oxidation of NADH at 340 nm in 3 mL cuvettes. The reaction contained HEPES buffer (pH 8.0), 6 mM $MgSO_4$, 25 mM NH_4Cl,

5 mM dithiothreitol, 0.1 mM disodium pyrophosphate, 0.25 mM AMP, 0.1 mM phosphoenolpyruvate, and 0.05-0.25 mg of *Blastocystis* cell-free extract or fraction. The rate of pyruvate production was determined by the addition of 2 U of lactate dehydrogenase and 0.25 mM NADH, and compared to controls with phosphoenolpyruvate but lacking AMP, and those containing AMP but lacking phosphoenolpyruvate. The concentration of AMP, pyrophosphate and phosphoenolpyruvate used in the assay was selected from preliminary assays using varying concentrations from 0.025-1.0 mM. The generation of ATP from AMP by pyruvate phosphate dikinase was confirmed by measuring the ATP formed using a luciferin/luciferse assay (Molecular Probes, In Vitrogen, Eugene, OR, USA). The assay was performed as described above but lacking lactate dehydrogenase and NADH, after varying times 0, 15, 30, 45 and 60 min 0.1 mL of the assay is removed and added to one well of a 96 well plate containing 0.1 mL of 0.25 μg firefly luciferase and 0.5 mM luciferin and the luminescence recorded using a Spectra Max M2 plate reader (Molecular Devices, Sunnyvale, CA).

The activity of pyrophosphate dependent phosphofructokinase* in the direction of fructose-1,6-bisphosphate formation (forward reaction) was determined in 1 mL assay volumes containing 0.1 M HEPES-HCl, pH 7.8; 20 mM fructose-6-phosphate; 2 mM Na pyrophosphate; 5 mM $MgCl_2$; 0.25 mM NADH; 0.2 U of aldolase (from rabbit muscle); and 0.3 U each of glycerophosphate dehydrogenase (from rabbit muscle) and triosephosphate isomerase (from rabbit muscle), 10 μM fructose 2,6 diphosphate. The reaction was initiated by addition of 0.05-0.25 mg of *Blastocystis* cell-free extract or fraction, and the rate of NADH oxidation was followed at 340 nm on a Beckman DU 640 spectrophotometer (Indianapolis, IN, USA). The activity of the reverse reaction was determined by measuring orthophosphate-dependent formation of fructose-6-phosphate from fructose-1,6-bisphosphate. The reaction mixture (1 mL) contained 0.1 M HEPES-HCl, pH 7.8; 2 mM fructose-1,6-bisphosphate; 15 mM NaH2PO4; 5 mM MgCl2; 0.3 mM $NADP^+$ and 0.12 U glucose- 6-phosphate dehydrogenase and 0.24 U glucose phosphate isomerase. The reaction was initiated by addition of 1 mg of pyrophosphate dependent phosphofructokinase and monitored at 340 nm. *Pyrophosphate fructose-6-phosphate 1-phosphotransferase (PFP).

Phylogenetic analyses

Sequences were automatically added to pre-existing alignments and subsequently manually refined using the Edit option of the MUST package (Philippe 1993). Final datasets were generated after elimination of highly variable regions and positions with more than 50% gaps by G-blocks (Talavera and Castresana

2007). All datasets were first analysed with a maximum likelihood (ML) method under two different models. PhyML v2.3 (Guindon and Gascuel 2003) was used with the SPR moves option and the LG+F+4G model (Le, et al. 2008) and PhyML v3 (with SPR moves) was used using the C20+4G model, corresponding to 20 pre-calculated fixed profiles of positional amino-acid substitution (Le, et al. 2008). Based on the likelihood values (l), the number of parameters (K) and alignment positions (n), the AIC (AIC= -2l +2K) and the corrected AIC (AICc; AIC+ 2K(K+1)/n-K-1) was calculated (Posada and Buckley 2004). The lowest AICc value corresponds to the best tree, if the value of the C20 analysis was better, then a second ML analysis under the C40+4G model was performed and the AICc value estimated, until the overall best model was found. If the AICc of C40 is better than C20 then C60 was tested. Once the best model was estimated for all six datasets, a rapid bootstrap analysis with 100 replicates in RAxML v7 under the LG model was performed (Stamatakis, et al. 2008) and an additional analysis in Phylobayes v3 with the CATfix C20 model in all cases or, alternatively, the best C-model. Two independent chains were run for 10,000 points and trees are sampled at every tenth points (Lartillot, et al. 2009). Trees obtained with the best model are presented and both posterior probabilities (PP) and rapid bootstrap values (BS) are indicated on trees if PP>0.5 or BS >30%, respectively.

Cellular localisation predictions

TargetP (Emanuelsson, et al. 2007) and MitoProt (Claros and Vincens 1996) were used to analyse putative subcellular localization. Non-plant and no cut-offs settings were used. However, in case of Viridiplantae, Rhodophyta and Glaucocystophyta, the plant settings were used if non-plant results differ. As stramenopiles contain plastids that arose via secondary endosymbiosis, their plastids are contained within the ER and proteins destined for the plastid contain an initial signal peptide. This generally results in erroneous predictions if plant settings are used (Gruber and Kroth 2014, 2017).

Results

When assembling the genome of the intestinal parasite *Blastocystis* (Gentekaki, et al. 2017), we discovered putative mitochondrial targeting signals on phosphoglycerate kinase (PGK) as well as on a fusion protein of triose phosphate isomerase (TPI) and glyceraldehyde phosphate dehydrogenase (GAPDH). The amino-terminal sequences conform to typical mitochondrial targeting signals and are enriched in alanine, leucine, serine and arginine (Neupert and Herrmann 2007) and are easily predicted

by programmes such as MitoProt (Claros and Vincens 1996). Analyses of the *Blastocystis* TPI-GAPDH and PGK sequences predicts a mitochondrial localisation of these proteins with high probabilities (P 0.99 and 0.97, respectively). The predicted cleavage sites coincide with the start of the cytosolic enzymes from other organisms (Fig. 1A) suggesting that these amino-terminal sequences might target both proteins to the unusual mitochondrial organelle in this parasite.

In order to test whether these predicated targeting signals are genuinely capable of guiding a protein to the mitochondria, we decided to try to target a reporter protein to these organelles. The predicted targeting signals were cloned in-frame upstream of the amino-terminus of the green fluorescent protein (GFP). The targeting constructs were used to transform *Phaeodactylum tricornutum*, a heterologous stramenopile alga and model system for stramenopile targeting (Gruber, et al. 2007). The GFP reporter protein was targeted to discrete locations in the *Phaeodactylum* cells, typical of mitochondria in this diatom (see Ewe, et al. 2018 for typical organellar localisations in *Phaeodactylum*; Gruber, et al. 2015) (Fig. 2A). This suggests that these putative targeting signals are functional and sufficient to target a reporter protein to mitochondria of a heterologous host.

As heterologous targeting is not evidence that these proteins are actually localised in the mitochondrial organelles of its homologous host *Blastocystis*, we raised antibodies against both TPI-GAPDH and PGK. When these homologous antibodies were used together, it was clear that both TPI-GAPDH and PGK localise to the same structures in *Blastocystis* and the scatterplot analysis provides a clear quantitative measure of signal overlap (Fig. 3 A-D). To demonstrate these structures were the mitochondria in this organism, we used the PGK antibody together with the mitochondria-specific dye MitoTracker and the DNA dye DAPI. Both MitoTracker and DAPI have been used to label *Blastocystis* mitochondria previously (Stechmann, et al. 2008). It is clear that PGK localises to the same structures as MitoTracker and DAPI (Fig. 3 E-I). The compartmentalised distribution of both TPI-GAPDH and PGK was clearly demonstrated in *Blastocystis* using confocal microscopy and three-dimensional rendering of optical sections confirming the mitochondrial localization of these glycolytic enzymes in this organism.

The unexpected mitochondrial localisation of these three glycolytic enzymes in *Blastocystis* prompted us to check all glycolytic enzymes in this intestinal parasite for possible mitochondrial targeting signals. Interestingly, targeting signals were only observed on the enzymes that are involved in the pay-off phase of glycolysis but not in the investment phase (Fig. 4).

Although three-dimensional reconstruction of our confocal microscopy data strongly indicated that these enzymes are indeed localised inside *Blastocystis* mitochondria (Fig. 3), we additionally decided to thoroughly confirm these findings using classical enzyme assays following cellular fractionation. *Blastocystis* cells were broken and subsequently separated using differential centrifugations into nuclear, mitochondrial, lysosomal and cytosolic fractions. Fractions were subsequently used in biochemical enzyme assays. These assays clearly showed that the activities of the five C3 enzymes are found in the mitochondrial pellet while the five enzymes upstream in glycolysis are all confined to the soluble fraction (Table 1). As it might be possible that the glycolytic enzymes were only attached to the surface of the mitochondria, as for instance in the case of hexokinase which is attached to the voltage-dependent anion channel (VDAC) in tumours (Lunt and Vander Heiden 2011), we tested the latency of enzymatic activities in the presence or absence of Triton X-100. The increase of measurable activity of the C3 but not the C6 glycolytic enzymes in the presence of detergent (Table 2) strongly indicates the C3 enzymes are indeed retained within a membranous compartment.

When proteolytic enzymes were used it was clear that these only affected the measured activity in the presence of the detergent Triton X-100 (Table 3). This clearly demonstrates that the five C3 glycolytic enzymes in *Blastocystis* are protected by a membrane and reside inside the mitochondria and not on the outside of the organelle, as observed in certain tumours (Lunt and Vander Heiden 2011) or some proteomics studies (Giege, et al. 2003; but see Smith, et al. 2007). This is the first genuine confirmation of true glycolytic enzyme activity inside mitochondria.

As some of us previously reported the mitochondrial localisation of the TPI-GAPDH fusion protein in a related stramenopile (Liaud, et al. 2000), we wondered whether mitochondrial targeting of glycolytic enzymes is more widespread in this group of organisms. When querying other stramenopile genomes, we noticed the widespread presence of mitochondrial targeting signals on glycolytic enzymes within the whole group. Here, as with *Blastocystis*, only enzymes of the C3 part of glycolysis contain mitochondrial targeting signals (Fig. 1B and Fig. 4).

To test for functionality, we also tested all predicted mitochondrial targeting signals from *Phaeodactylum* C3 glycolytic enzymes. The targeting signals were fused to GFP and their cellular location was determined (Fig. 2B). As with *Blastocystis*, all constructs were targeted to the mitochondria suggesting these are genuine mitochondrial targeting signals *in vivo*. In addition, we also tested mitochondrial targeting signals found on glycolytic enzymes of the oomycete pathogen *Phytophthora infestans*, the water mould *Achlya bisexualis* and the multicellular brown alga *Saccharina latissima*, commonly known

as kelp (Fig. 2C). In all cases, these targeting signals targeted GFP into the mitochondria of the diatom suggesting that mitochondrial localisation of the C3 part of glycolysis is a more general feature in the stramenopiles. However, for some organisms we also detected non-targeting signal bearing glycolytic enzymes suggesting that these cells possibly have a branched glycolytic pathway (see Fig. 5 and 6).

The mitochondrial proteome has a complex and contested evolutionary past (Ku, et al. 2015; Martin, et al. 2017; Pittis and Gabaldon 2016; van der Giezen 2011), and we wondered if glycolytic enzymes targeted to mitochondria might have different evolutionary origins than those that operate in the cytosol. Sequences of all glycolytic enzymes from *Phaeodactylum tricornutum* and *Blastocystis* ST1, strain NandII, were used as seeds in BlastP searches in the non-redundant database at the NCBI (Altschul, et al. 1990). We were especially interested to identify all sequences in the SAR supergroup (Adl, et al. 2012) (Stramenopiles, Alveolates and Rhizaria). In addition, representatives from other eukaryotic groups and, if required, closely related bacterial sequences were added. Phylogenetic analysis of all glycolytic enzymes does not seem to be able to support either hypothesis of different evolutionary origins of cytosolic versus mitochondrial glycolytic enzymes (Supplementary Figure S1 A-F).

Discussion

Eukaryotes evolved from a symbiosis between an archaeal host and a bacterial endosymbiont that became the mitochondrion (Martin, et al. 2015; van der Giezen 2011). Although many different hypotheses have been posited over the years, they principally boil down to two scenarios. The phagotropic origin of eukaryotes suggests they evolved gradually from a less complex prokaryote and once phagotrophy had evolved, the mitochondrial endosymbiosis was possible (see O'Malley 2010). The syntrophic eukaryotic origin suggests the establishment of the mitochondrial endosymbiont was the same event as the origin of eukaryotes (see Martin, et al. 2015). Arguments have been put forward for and against either scenario and it seems that biochemical/physiological arguments favour a synthrophic origin and cell biological/morphological arguments favour a phagotrophic origin. Both scenarios seem to agree that the host was archaeal and the endosymbiont bacterial (Martin, et al. 2015; Roger, et al. 2017). The subsequent replacement of the host's gene repertoire encoding metabolic capacity has been explained by endosymbiotic gene transfer (reviewed in Timmis, et al. 2004) and the resulting chimeric nature of eukaryotes had been noticed earlier (Rivera, et al. 1998). The nature of the mitochondrial endosymbiont has long been understood to be alpha-proteobacterial (Gupta 1995) but only recently have studies zoomed in on the more precise affiliations of the archaeal host (Cox, et al. 2008; Eme, et al. 2017; Martin,

et al. 2015; Williams, et al. 2013; Zaremba-Niedzwiedzka, et al. 2017). A recent study suggests that mitochondria are perhaps ancestral to alpha-proteobacteria, but does not exclude an alpha-proteobacterial origin (Martijn, et al. 2018). A few billion years of independent evolution of the endosymbiont's lineage and widespread bacterial lateral gene transfer (even predating the mitochondrial symbiosis) can explain that not all eukaryotic metabolic proteins have a clear alpha-proteobacterial evolutionary signal. Despite all this, glycolytic enzymes of eukaryotes do all cluster with bacterial homologues in phylogenetic trees (Supplementary Figure S1; Esser, et al. 2004; Martin, et al. 1993; Martin and Herrmann 1998)). It is indeed implicit of eukaryotic origin theories (Martin and Müller 1998; Martin, et al. 2015) that glycolysis was originally acquired from the mitochondrial endosymbiont. It is therefore interesting to consider whether the mitochondrial targeting of glycolytic enzymes in stramenopiles represents an ancestral or a derived state for eukaryotes. The deep branches of the eukaryotic tree are not known with certainty, but there is substantial phylogenomic support for the grouping of stramenopiles with alveolates and rhizarians to form the "SAR" supergroup (Burki, et al. 2008). Intriguingly, predicted mitochondrial targeting has been reported for several glycolytic enzymes – including TPI-GAPDH fusion proteins – in members of the cercozoa, a group of rhizarians (Nakayama, et al. 2012); the distantly-related apusozoan *Thecamonas trahens* also encodes a TPI-GAPDH fusion protein (Nakayama, et al. 2012). Taken together, these data raise the possibility that at least some of the latter steps of glycolysis may have occurred in the mitochondria of the SAR common ancestor (Nakayama, et al. 2012). However, these inferences are currently based on a very limited sample of SAR diversity, and testing hypotheses about the localisation of glycolysis in early eukaryotes will require both more genomes and more of the experimental characterisation that we report here.

Evolution of mitochondrial protein targeting was a requirement for the successful integration of the mitochondrial endosymbiont and should have happened at least concomitant with endosymbiotic gene transfer if those gene products had to function in the newly formed organelle (comparison to more recently evolved host/symbiont systems suggests that the first proteins that are targeted to an endosymbiont in fact do not originate from the endosymbiont and that the evolution of protein targeting precedes the direct transfer of endosymbiont genes to the host nucleus (Nowack 2014)). Mitochondrial targeting signals do not conform to a strict consensus sequence and secondary structure is a key factor in their functionality (Schatz and Dobberstein 1996). These pre-sequences form amphipathic alpha helices with alternating hydrophobic and positively charged amino acids (Allison and Schatz 1986; Roise, et al. 1988; von Heijne 1986). Mitochondrial targeting sequences can arise randomly (Baker and Schatz 1987), exist in bacteria (Lucattini, et al. 2004) and can be acquired by DNA recombination or exon shuffling (Kubo,

et al. 1999; Long, et al. 1996; Wischmann and Schuster 1995). The predicted pre-sequences for the stramenopiles are in the size range of known mitochondrial targeting signals (von Heijne, et al. 1989) and are also enriched in alanine, leucine, serine and arginine (Neupert and Herrmann 2007). Organellar targeting signals for mitochondrial remnants such as the mitochondrial organelle in *Blastocystis* tend to be shorter than but not as short as those found for *Trichomonas* hydrogenosomes (Garg, et al. 2015; van der Giezen, et al. 2005). However, there do seem to be some characteristic features even for these hydrogenosomal pre-sequences with often a leucine at the second position and an arginine two places before the cleavage site (Bradley, et al. 1997; van der Giezen, et al. 1998).

It is difficult to conclusively determine the selective advantage, if any, for the retargeting or the conservation of glycolysis to/in stramenopile mitochondria. In *Blastocystis*, similar to many parasitic eukaryotes (Mertens 1993), two key glycolytic enzymes have been replaced by pyrophosphate using versions. Normally, the reactions catalysed by phosphofructokinase and pyruvate kinase are virtually irreversible. However, the reactions performed by diphosphate-fructose-6-phosphate 1-phosphotransferase and phosphoenolpyruvate synthase (pyruvate, water dikinase) are reversible, due to the smaller free-energy change in the reaction. As *Blastocystis* is an anaerobe and does not contain normal mitochondrial oxidative phosphorylation (Gentekaki, et al. 2017; Stechmann, et al. 2008), any ATP not invested during glycolysis might be a selective advantage. However, in the absence of these irreversible control points there is a risk of uncontrolled glycolytic oscillations (Chandra, et al. 2011). Separating the investment phase from the pay-off phase by the mitochondrial membranes might therefore prevent futile cycling. However, as not all stramenopiles use pyrophosphate enzymes, this cannot be the whole explanation.

Similarly to the peculiarity of pyrophosphate utilization in *Blastocystis*, diatoms also show metabolic peculiarities that are not shared with other organisms (Gruber and Kroth 2017). One such peculiarity is the presence of an Entner-Doudoroff pathway in the mitochondria of *P. tricornutum* (Fabris, et al. 2012). This pathway, like glycolysis, degrades glucose to pyruvate. However, the net ATP yield of the Entner-Doudoroff pathway is lower (one ATP per glucose) and the two reducing equivalents that are formed are one NADH and one NADPH per glucose. The degradation of glyceraldehyde 3-phosphate in the Entner-Doudoroff pathway uses identical reaction steps as the glycolysis. Mitochondrial glycolysis therefore might be a complement of the mitochondrial Entner-Doudoroff pathway in *P. tricornutum* (and other photosynthetic stramenopiles with an Entner-Doudoroff pathway) (Fabris, et al. 2012). However, we did

not find evidence for an Entner-Doudoroff pathway in non-photosynthetic stramenopiles, so again, this explanation might not be valid for all stramenopiles with mitochondrial glycolysis.

Glycolysis depends on recycling of the reducing equivalents that are formed in the GAPDH reaction (in which NAD^+ is reduced to NADH). To keep the reactions going, NAD^+ needs to be regenerated. How this is done depends on the presence of oxygen. Under anoxic conditions, pyruvate usually is reduced in a fermentation reaction which recovers oxidised NAD^+ (most commonly lactic acid or ethanol fermentation). Under aerobic conditions, the reducing equivalents are transferred to O_2 in the mitochondrial respiratory electron transport chain. In organisms that operate glycolysis exclusively in the cytosol, NAD^+/NADH apparently cannot be transported directly into mitochondria. Instead two shuttle systems, the glycerol phosphate shuttle and the malate-aspartate shuttle, lead to indirect exchange of reducing equivalents between cytosol and mitochondria. To release reducing equivalents directly in the mitochondrial matrix where they can be accepted by the respiratory electron transport chain without the need of a shuttle system seems an elegant solution. Similarly, if the redox shuttle system between cytosol and mitochondrial matrix is absent, it also makes sense that the NADPH generating glucose-6-phosphate-dehydrogenase reaction in the above mentioned Entner-Doudoroff pathway in photosynthetic stramenopiles takes place in the mitochondria.

The malate-aspartate shuttle requires a cytosolic malate dehydrogenase (MDH). *P. tricornutum* does not possess a cytosolic MDH (Ewe, et al. 2018), which might also suggest an absence of a malate-aspartate shuttle in this diatom. However, if difficulties in redox shuttling would require the redox reactive steps to occur in the mitochondria, this would not explain mitochondrial glycolysis in *Blastocystis*, an organism that does not rely on oxidative ATP generation. Furthermore, physiological data suggests that in diatoms, considerable shuttling of reducing equivalents from the plastid to the mitochondria may occur as a measure to prevent the formation of reactive oxygen species at the photosystems when excessive excitation energy is absorbed (Allen, et al. 2008; Bailleul, et al. 2015). These findings, and also the presence of unusual transport proteins for nucleotides (Ast, et al. 2009; Chu, et al. 2017), do not support the hypothesis of a lack of efficient shuttling, but underline the importance of stramenopile mitochondria as electron sinks in the recycling of electron acceptors that are reduced either in the mitochondria (in the mitochondrial pay-off phase of glycolysis or in the above-mentioned Entner–Doudoroff pathway) or in other compartments (in the cytosolic part of glycolysis or in the photosynthetic electron transport chain in the plastids).

Recently, Abrahamian *et al* (2017) reported similar findings to ours and used GFP-tagged proteins in *P. infestans* to demonstrate the mitochondrial localization of glycolytic enzymes. They also report the targeting of several steps of a serine anabolic pathway to *P. infestans* mitochondria and suggested the shared 3-phosphoglycerate intermediate would be the *raison d'être* for the mitochondrial glycolysis (Abrahamian, et al. 2017).

All the points discussed above might indeed provide several possible physiological explanations for the observed mitochondrial glycolysis in stramenopiles, but unfortunately do not answer the question whether mitochondrial glycolysis is a primary or secondary state in these group of eukaryotes.

The end-product of glycolysis, pyruvate, is transported into mitochondria via a specific mitochondrial transporter that has only recently been identified (Herzig, et al. 2012) and that is absent from the *Blastocystis* genome (Gentekaki, et al. 2017). The translocation of the C3 part of glycolysis into mitochondria would necessitate a novel transporter (presumably for triose phosphates). The identification and characterisation of such a transporter would open up new possible drug targets against important pathogens. Examples include *Phytophthora infestans*, the causative agent of late potato blight, which has a devastating effect on food security, but also fish parasites such as *Saprolegnia parasitica* and *Aphanomyces invadans.* Both have serious consequences for aquaculture and the latter causes epizootic ulcerative syndrome, an OIE listed disease (Jiang and Tyler 2012; Stentiford, et al. 2014). Our recent genome analysis of *Blastocystis* identified several putative candidate transporters lacking clear homology to non-stramenopile organisms (Gentekaki, et al. 2017). Such a unique transporter would not be present in the host (including humans) and could be exploited to prevent, or control, disease outbreaks that currently affect food production while the world population continuous to increase (FAO 2009).

Conclusion

Taken together, our results show that glycolysis, contrary to the textbook view on well-investigated model organisms, not only occurs in the cytosol, but also occurs in the mitochondria. All tested stramenopiles show evidence of the second half of glycolysis taking place in the mitochondria and the cytosol, with the exception of the human pathogen *Blastocystis*, in which the second half of glycolysis occurs exclusively in the mitochondria. Mitochondrial glycolysis therefor seems to be a common feature of the stramenopiles, despite the considerable metabolic and physiological diversity within this group. Although it remains unclear whether this feature is ancestral or derived, our findings show that the

intracellular distribution of even the most basic metabolic pathways is variable between the different groups of eukaryotes.

Acknowledgements

The authors wish to thank Professors John F. Allen and Nick Lane (both University College London, UK) for fruitful discussions and criticism. We also like to thank the two reviewers for their suggestions. Furthermore, we want to thank Ulrike Brand (Technische Universität Braunschweig, TU-BS) and Doris Ballert (University of Konstanz) for technical assistance, the BioImaging Center of the University of Konstanz for access to confocal microscopes as well as Professor Ralf-Rainer Mendel and his group (TU-BS) for sharing equipment. TAW is supported by a Royal Society University Research Fellowship and NERC grant NE/P00251X/1. Work in the lab of MvdG was supported by Wellcome Trust grant 078566/A/05/Z. PGK wishes to acknowledge support by the German Research Foundation (DFG, grant KR 1661/6-1) and the Gordon and Betty Moore Foundation GBMF 4966 (grant DiaEdit).

Literature cited

Abrahamian M, Kagda M, Ah-Fong AMV, Judelson HS 2017. Rethinking the evolution of eukaryotic metabolism: novel cellular partitioning of enzymes in stramenopiles links serine biosynthesis to glycolysis in mitochondria. BMC Evolutionary Biology 17: 241. doi: 10.1186/s12862-017-1087-8
Adl SM, et al. 2012. The revised classification of eukaryotes. J Eukaryot Microbiol 59: 429-493. doi: 10.1111/j.1550-7408.2012.00644.x
Allen AE, et al. 2008. Whole-cell response of the pennate diatom *Phaeodactylum tricornutum* to iron starvation. Proc Natl Acad Sci U S A 105: 10438-10443. doi: 10.1073/pnas.0711370105
Allison DS, Schatz G 1986. Artificial mitochondrial presequences. Proc Natl Acad Sci U S A 83: 9011-9015.
Altschul SF, Gish W, Miller W, Myers EW, Lipman DJ 1990. Basic local alignment search tool. J. Mol. Biol. 215: 403-410.
Ast M, et al. 2009. Diatom plastids depend on nucleotide import from the cytosol. Proc Natl Acad Sci U S A 106: 3621-3626. doi: 10.1073/pnas.0808862106
Bailleul B, et al. 2015. Energetic coupling between plastids and mitochondria drives CO2 assimilation in diatoms. Nature 524: 366-369. doi: 10.1038/nature14599
Baker A, Schatz G 1987. Sequences from a prokaryotic genome or the mouse dihydrofolate reductase gene can restore the import of a truncated precursor protein into yeast mitochondria. Proc Natl Acad Sci U S A 84: 3117-3121.
Baurain D, et al. 2010. Phylogenomic evidence for separate acquisition of plastids in cryptophytes, haptophytes, and stramenopiles. Mol Biol Evol 27: 1698-1709. doi: 10.1093/molbev/msq059
Bhattacharya D, Stickel SK, Sogin ML 1991. Molecular phylogenetic analysis of actin genic regions from *Achlya bisexualis* (Oomycota) and *Costaria costata* (Chromophyta). J Mol Evol 33: 525-536.

Bowler C, et al. 2008. The *Phaeodactylum* genome reveals the evolutionary history of diatom genomes. Nature 456: 239-244.
Bradley PJ, Lahti CJ, Plümper E, Johnson PJ 1997. Targeting and translocation of proteins into the hydrogenosome of the protist *Trichomonas*: similarities with mitochondrial protein import. EMBO J. 16: 3484-3493.
Burki F, Shalchian-Tabrizi K, Pawlowski J 2008. Phylogenomics reveals a new 'megagroup' including most photosynthetic eukaryotes. Biology Letters 4: 366-369.
Chandra FA, Buzi G, Doyle JC 2011. Glycolytic oscillations and limits on robust efficiency. Science 333: 187-192. doi: 10.1126/science.1200705
Chu L, et al. 2017. Shuttling of (deoxy-) purine nucleotides between compartments of the diatom *Phaeodactylum tricornutum*. New Phytol 213: 193-205. doi: 10.1111/nph.14126
Claros MG, Vincens P 1996. Computational method to predict mitochondrially imported proteins and their targeting sequences. Eur. J. Biochem. 241: 779-786.
Cox CJ, Foster PG, Hirt RP, Harris SR, Embley TM 2008. The archaebacterial origin of eukaryotes. Proc Natl Acad Sci U S A 105: 20356-20361.
Derelle R, López-García P, Timpano H, Moreira D 2016. A phylogenomic framework to study the diversity and evolution of stramenopiles (=heterokonts). Molecular Biology and Evolution 33: 2890-2898. doi: 10.1093/molbev/msw168
Emanuelsson O, Brunak S, von Heijne G, Nielsen H 2007. Locating proteins in the cell using TargetP, SignalP and related tools. Nat Protoc 2: 953-971. doi: 10.1038/nprot.2007.131
Eme L, Spang A, Lombard J, Stairs CW, Ettema TJG 2017. Archaea and the origin of eukaryotes. Nat Rev Microbiol 15: 711-723. doi: 10.1038/nrmicro.2017.133
Esser C, et al. 2004. A genome phylogeny for mitochondria among alpha-proteobacteria and a predominantly eubacterial ancestry of yeast nuclear genes. Mol Biol Evol 21: 1643-1660.
Ewe D, et al. 2018. The intracellular distribution of inorganic carbon fixing enzymes does not support the presence of a C4 pathway in the diatom *Phaeodactylum tricornutum*. Photosynth Res. doi: 10.1007/s11120-018-0500-5
Fabris M, et al. 2012. The metabolic blueprint of *Phaeodactylum tricornutum* reveals a eukaryotic Entner-Doudoroff glycolytic pathway. Plant J 70: 1004-1014. doi: 10.1111/j.1365-313X.2012.04941.x
FAO. 2009. How to feed the world in 2050. In: Food and Agriculture Organization of the United Nations (FAO).
Freitag J, Ast J, Bolker M 2012. Cryptic peroxisomal targeting via alternative splicing and stop codon read-through in fungi. Nature 485: 522-525.
Garg S, et al. 2015. Conservation of transit peptide-independent protein import into the mitochondrial and hydrogenosomal matrix. Genome Biol Evol 7: 2716-2726. doi: 10.1093/gbe/evv175
Gentekaki E, et al. 2017. Extreme genome diversity in the hyper-prevalent parasitic eukaryote *Blastocystis*. PLoS Biol 15: e2003769.
Giege P, et al. 2003. Enzymes of glycolysis are functionally associated with the mitochondrion in *Arabidopsis* cells. Plant Cell 15: 2140-2151.
Gruber A, Kroth PG 2014. Deducing intracellular distributions of metabolic pathways from genomic data. Methods Mol Biol 1083: 187-211. doi: 10.1007/978-1-62703-661-0_12
Gruber A, Kroth PG 2017. Intracellular metabolic pathway distribution in diatoms and tools for genome-enabled experimental diatom research. Philos Trans R Soc Lond B Biol Sci 372. doi: 10.1098/rstb.2016.0402
Gruber A, Rocap G, Kroth PG, Armbrust EV, Mock T 2015. Plastid proteome prediction for diatoms and other algae with secondary plastids of the red lineage. Plant J 81: 519-528. doi: 10.1111/tpj.12734
Gruber A, et al. 2007. Protein targeting into complex diatom plastids: functional characterisation of a specific targeting motif. Plant Mol Biol 64: 519-530. doi: 10.1007/s11103-007-9171-x

Guindon S, Gascuel O 2003. A simple, fast, and accurate algorithm to estimate large phylogenies by maximum likelihood. Syst. Biol. 52: 696-704.
Gupta RS 1995. Evolution of the chaperonin families (Hsp60, Hsp10 and Tcp-1) of proteins and the origin of eukaryotic cells. Mol. Microbiol. 15: 1-11.
Herzig S, et al. 2012. Identification and functional expression of the mitochondrial pyruvate carrier. Science 337: 93-96.
Jiang RH, Tyler BM 2012. Mechanisms and evolution of virulence in oomycetes. Annu Rev Phytopathol 50: 295-318. doi: 10.1146/annurev-phyto-081211-172912
Keeling PJ, et al. 2010. The reduced genome of the parasitic microsporidian *Enterocytozoon bieneusi* lacks genes for core carbon metabolism. Genome Biol Evol 2: 304-309.
Kroth P 2007. Genetic transformation - a tool to study protein targeting in diatoms. Methods in Molecular Biology 390: 257-268.
Kroth PG, et al. 2008. A model for carbohydrate metabolism in the diatom Phaeodactylum tricornutum deduced from comparative whole genome analysis. PLoS ONE 3: e1426. doi: 10.1371/journal.pone.0001426
Ku C, et al. 2015. Endosymbiotic origin and differential loss of eukaryotic genes. Nature 524: 427-432. doi: 10.1038/nature14963
Kubo N, Harada K, Hirai A, Kadowaki K 1999. A single nuclear transcript encoding mitochondrial RPS14 and SDHB of rice is processed by alternative splicing: common use of the same mitochondrial targeting signal for different proteins. Proc Natl Acad Sci U S A 96: 9207-9211.
Lartillot N, Lepage T, Blanquart S 2009. PhyloBayes 3: a Bayesian software package for phylogenetic reconstruction and molecular dating. Bioinformatics 25: 2286-2288. doi: 10.1093/bioinformatics/btp368
Le SQ, Lartillot N, Gascuel O 2008. Phylogenetic mixture models for proteins. Philos Trans R Soc Lond B Biol Sci 363: 3965-3976. doi: 10.1098/rstb.2008.0180
Liaud MF, Brandt U, Scherzinger M, Cerff R 1997. Evolutionary origin of cryptomonad microalgae: two novel chloroplast/cytosol-specific GAPDH genes as potential markers of ancestral endosymbiont and host cell components. J Mol Evol 44 Suppl 1: S28-37.
Liaud MF, Lichtle C, Apt K, Martin W, Cerff R 2000. Compartment-specific isoforms of TPI and GAPDH are imported into diatom mitochondria as a fusion protein: evidence in favor of a mitochondrial origin of the eukaryotic glycolytic pathway. Mol Biol Evol 17: 213-223.
Lill R, et al. 1999. The essential role of mitochondria in the biogenesis of cellular iron-sulfur proteins. Biol. Chem. 380: 1157-1166.
Long M, de Souza SJ, Rosenberg C, Gilbert W 1996. Exon shuffling and the origin of the mitochondrial targeting function in plant cytochrome c1 precursor. Proc Natl Acad Sci U S A 93: 7727-7731.
Lucattini R, Likic VA, Lithgow T 2004. Bacterial proteins predisposed for targeting to mitochondria. Mol Biol Evol 21: 652-658. doi: 10.1093/molbev/msh058
Lunt SY, Vander Heiden MG 2011. Aerobic glycolysis: meeting the metabolic requirements of cell proliferation. Annu Rev Cell Dev Biol 27: 441-464. doi: 10.1146/annurev-cellbio-092910-154237
Maheswari U, et al. 2005. The Diatom EST Database. Nucleic Acids Res 33: D344-347. doi: 10.1093/nar/gki121
Martijn J, Vosseberg J, Guy L, Offre P, Ettema TJG 2018. Deep mitochondrial origin outside the sampled alphaproteobacteria. Nature 557: 101-105. doi: 10.1038/s41586-018-0059-5
Martin W, Brinkmann H, Savonna C, Cerff R 1993. Evidence for a chimeric nature of nuclear genomes: eubacterial origin of eukaryotic glyceraldehyde-3-phosphate dehydrogenase genes. Proc Natl Acad Sci U S A 90: 8692-8696.
Martin W, Herrmann RG 1998. Gene transfer from organelles to the nucleus: how much, what happens, and Why? Plant Physiol 118: 9-17.
Martin W, Müller M 1998. The hydrogen hypothesis for the first eukaryote. Nature 392: 37-41.

Martin WF, Garg S, Zimorski V 2015. Endosymbiotic theories for eukaryote origin. Philos Trans R Soc Lond B Biol Sci 370: 20140330. doi: 10.1098/rstb.2014.0330
Martin WF, et al. 2017. Late mitochondrial origin is an artifact. Genome Biol Evol 9: 373-379. doi: 10.1093/gbe/evx027
Mertens E 1993. ATP versus pyrophosphate: glycolysis revisited in parasitic protists. Parasitol Today 9: 122-126.
Morales J, et al. 2016. Differential remodelling of peroxisome function underpins the environmental and metabolic adaptability of diplonemids and kinetoplastids. Proceedings of the Royal Society B: Biological Sciences 283. doi: 10.1098/rspb.2016.0520
Müller M, et al. 2012. Biochemistry and evolution of anaerobic energy metabolism in eukaryotes. Microbiol Mol Biol Rev 76: 444-495.
Nakayama T, Ishida K, Archibald JM 2012. Broad distribution of TPI-GAPDH fusion proteins among eukaryotes: evidence for glycolytic reactions in the mitochondrion? PLoS ONE 7: e52340.
Neupert W, Herrmann JM 2007. Translocation of proteins into mitochondria. Annu Rev Biochem 76: 723-749.
Noel C, et al. 2005. Molecular phylogenies of *Blastocystis* isolates from different hosts: implications for genetic diversity, identification of species, and zoonosis. J Clin Microbiol 43: 348-355. doi: 10.1128/JCM.43.1.348-355.2005
Nowack ECM 2014. *Paulinella chromatophora* - rethinking the transition from endosymbiont to organelle. Acta Societatis Botanicorum Poloniae 83: 387-397.
O'Malley MA 2010. The first eukaryote cell: an unfinished history of contestation. Stud Hist Philos Biol Biomed Sci 41: 212-224. doi: S1369-8486(10)00044-0 [pii]

10.1016/j.shpsc.2010.07.010
Opperdoes FR, Borst P 1980. Localization of nine glycolytic enzymes in a microbody-like organelle in *Trypanosoma brucei*: the glycosome. FEBS Lett 80: 360-364.
Petersen J, et al. 2014. Chromera velia, endosymbioses and the rhodoplex hypothesis--plastid evolution in cryptophytes, alveolates, stramenopiles, and haptophytes (CASH lineages). Genome Biol Evol 6: 666-684. doi: 10.1093/gbe/evu043
Philippe H 1993. MUST, a computer package of management utilities for sequences and trees. Nucleic.Acids.Research. 21: 5264-5272.
Pittis AA, Gabaldon T 2016. Late acquisition of mitochondria by a host with chimaeric prokaryotic ancestry. Nature 531: 101-104. doi: 10.1038/nature16941
Posada D, Buckley TR 2004. Model selection and model averaging in phylogenetics: advantages of akaike information criterion and bayesian approaches over likelihood ratio tests. Syst Biol 53: 793-808. doi: 10.1080/10635150490522304
Rivera MC, Jain R, Moore JE, Lake JA 1998. Genomic evidence for two functionally distinct gene classes. Proc. Natl. Acad. Sci. USA 95: 6239-6244.
Roger AJ, Munoz-Gomez SA, Kamikawa R 2017. The origin and diversification of mitochondria. Curr Biol 27: R1177-R1192. doi: 10.1016/j.cub.2017.09.015
Roise D, et al. 1988. Amphiphilicity is essential for mitochondrial presequence function. EMBO Journal. 7: 649-653.
Sambrook J, Fritsch E, Maniatis T. 1989. Molecular cloning, a laboratory manual. New York, USA: Cold Spring Harbor Laboratory Press.
Schatz G, Dobberstein B 1996. Common principles of protein translocation across membranes. Science 271: 1519-1526.
Scheffler IE. 2008. Mitochondria. 2nd edition. Hoboken, New Jersey: J. Wiley and Sons, Inc.

Smith DG, et al. 2007. Exploring the mitochondrial proteome of the ciliate protozoon Tetrahymena thermophila: direct analysis by tandem mass spectrometry. J Mol Biol 374: 837-863.
Stamatakis A, Hoover P, Rougemont J 2008. A Rapid Bootstrap Algorithm for the RAxML Web Servers. Systematic Biology 57: 758-771. doi: 10.1080/10635150802429642
Stechmann A, et al. 2008. Organelles in *Blastocystis* that blur the distinction between mitochondria and hydrogenosomes. Curr Biol 18: 580-585.
Stensvold CR, et al. 2007. Terminology for *Blastocystis* subtypes - a consensus. Trends Parasitol 23: 93-96.
Stensvold CR, van der Giezen M 2018. Associations between gut microbiota and common luminal intestinal parasites. Trends Parasitol. doi: 10.1016/j.pt.2018.02.004
Stentiford GD, Feist SW, Stone DM, Peeler EJ, Bass D 2014. Policy, phylogeny, and the parasite. Trends Parasitol 30: 274-281. doi: 10.1016/j.pt.2014.04.004
Talavera G, Castresana J 2007. Improvement of phylogenies after removing divergent and ambiguously aligned blocks from protein sequence alignments. Syst Biol 56: 564-577. doi: 10.1080/10635150701472164
Timmis JN, Ayliffe MA, Huang CY, Martin W 2004. Endosymbiotic gene transfer: organelle genomes forge eukaryotic chromosomes. Nat Rev Genet 5: 123-135.
Tripathy S, Pandey VN, Fang B, Salas F, Tyler BM 2006. VMD: a community annotation database for oomycetes and microbial genomes. Nucleic Acids Res 34: D379-381. doi: 10.1093/nar/gkj042
Tyler BM, et al. 2006. *Phytophthora* genome sequences uncover evolutionary origins and mechanisms of pathogenesis. Science 313: 1261-1266. doi: 10.1126/science.1128796
van der Giezen M 2011. Mitochondria and the rise of eukaryotes. BioSci 61: 594-601.
van der Giezen M, Kiel JAKW, Sjollema KA, Prins RA 1998. The hydrogenosomal malic enzyme from the anaerobic fungus *Neocallimastix frontalis* is targeted to mitochondria of the methylotrophic yeast *Hansenula polymorpha*. Curr. Genet. 33: 131-135.
van der Giezen M, Tovar J, Clark CG 2005. Mitochondrion-derived organelles in protists and fungi. Int Rev Cytol 244: 175-225.
von Heijne G 1986. Mitochondrial targeting sequences may form amphiphilic helices. EMBO Journal. 5: 1335-1342.
von Heijne G, Steppuhn J, Herrmann RG 1989. Domain structure of mitochondrial and chloroplast targeting peptides. Eur. J. Biochem. 180: 535-545.
Walker G, Dorrell RG, Schlacht A, Dacks JB 2011. Eukaryotic systematics: a user's guide for cell biologists and parasitologists. Parasitology 138: 1638-1663. doi: 10.1017/S0031182010001708
Williams TA, Foster PG, Cox CJ, Embley TM 2013. An archaeal origin of eukaryotes supports only two primary domains of life. Nature 504: 231-236. doi: 10.1038/nature12779
Wiredu Boakye D, et al. 2017. Decay of the glycolytic pathway and adaptation to intranuclear parasitism within *Enterocytozoonidae microsporidia*. Environmental Microbiology 19: 2077-2089. doi: doi:10.1111/1462-2920.13734
Wischmann C, Schuster W 1995. Transfer of rps10 from the mitochondrion to the nucleus in *Arabidopsis thaliana*: evidence for RNA-mediated transfer and exon shuffling at the integration site. FEBS Lett 374: 152-156.
Zaremba-Niedzwiedzka K, et al. 2017. Asgard archaea illuminate the origin of eukaryotic cellular complexity. Nature 541: 353-358. doi: 10.1038/nature21031
Zaslavskaia LA, Lippmeier JC, Kroth PG, Grossman AR, Apt KE 2000. Transformation of the diatom *Phaeodactylum tricornutum* (Bacillariophyceae) with a variety of selectable marker and reporter genes. J. Phycol. 36: 379-386.

Tables

Table 1. Pay-off phase glycolytic enzymes in *Blastocystis* are found in the mitochondrial pellet. Activities of glycolytic enzymes from whole cell free extracts (c.f.e.) of *Blastocystis* suspended in phosphate buffered isotonic sucrose solution (pH 7.2). Cells were mixed at a ratio of two volumes of cells: three volumes of 0.5 mm glass beads and broken by three shakes of one minute each at maximum speed on a bead beater (VWR mini bead mill homogenizer (Atlanta, GA, USA)). Cell-free extracts were subjected to increasing centrifugal force producing nuclear, mitochondrial (pellet), lysosomal and cytosolic (supernatant) fractions at 1,912 RCF_{av} for 5 min, 6,723 RCF_{av} for 15 min, 26,892 RCF_{av} for 30 min, respectively. Enzyme activities are the average of three determinations ± SD. *1 enzyme unit (EU) is the amount of enzyme that converts 1 µmole substrate to product per minute. The yellow box indicates the site of major activity (or in the case of triosephosphate isomerase, the dual localization).

	c.f.e.	supernatant	pellet
hexokinase	9.3 ± 2.6	21.1 ± 3.6	2.3 ± 0.6
phosphoglucose isomerase	3.6 ± 0.8	5.8 ± 1.2	1.7 ± 0.4
(pyrophosphate-dependent) phosphofructokinase	11.2 ± 1.8	27.1 ± 3.2	2.4 ± 1.6
fructose bisphosphate aldolase	3.8 ± 1.3	10.9 ± 1.3	0.62 ± 0.3
triosephosphate isomerase	18.3 ± 3.1	36 ± 5.1	18.0 ± 2.8
glyceraldehyde phosphate dehydrogenase	9.2 ± 1.4	0.5 ± 0.1	54.7 ± 5.8
phosphoglycerate kinase	9.8 ± 1.7	5.3 ± 1.3	36.2 ± 4.1
phosphoglycerate mutase	1.2 ± 0.5	0.04 ± 0.01	2.6 ± 0.7
enolase	0.42 ± 0.1	0.37 ± 0.07	1.6 ± 0.4
pyruvate kinase/phosphoenolpyruvate synthase	2.8 ± 0.7	3.3 ± 0.10	15.4 ± 2.3

Table 2. Latency of ML organelles with respect to glycolytic enzymes.

Glycolytic enzymes localizing to the mitochondrial-like organelle were assayed in 225 mM sucrose buffered solutions complete with substrate(s) and monitored on a spectrophotometer for 15 min. Triton X-100 (0.1%) was added and the wavelength monitored for a further 15 min. Results are presented as the mean ± SD of triplicate experiments.

	control	Triton
glyceraldehyde phosphate dehydrogenase	8.5 ± 2.9	66 ± 12
phosphoglycerate kinase	3.8 ± 2.0	35 ± 13
phosphoglycerate mutase	0.5 ± 0.4	4.0 ± 0.9
enolase	0.2 ± 0.2	1.8 ± 0.5
phosphoenolpyruvate synthase	2.9 ± 1.6	26 ± 5.7

(1 µmol substrate to product per minute)

Table 3. *Blastocystis* glycolytic enzymes are protected by a membrane. Control: Mitochondrial fractions incubated without proteolytic enzymes. Protease: Mitochondria incubated in 225 mM sucrose buffer at 25 °C containing 500 U bovine pancreas trypsin, 10 U papaya latex papain and 250 U porcine pepsin for 15 minutes. Protease + Triton: Mitochondrial fractions containing proteolytic enzymes and 1% Triton X-100 incubated for 15 min at 25 °C. Samples were centrifuged (14,000 g) for 2 min and resuspended in fresh sucrose buffer without proteolytic enzymes prior to assay.

	control	protease	protease + Triton
glyceraldehyde phosphate dehydrogenase	71 ± 14	61 ± 9.1	15 ± 4.8
phosphoglycerate kinase	36 ± 8.5	33 ± 4.5	6.3 ± 2.2
phosphoglycerate mutase	4.0 ± 1.2	3.1 ± 0.5	0.2 ± 0.1
enolase	1.8 ± 0.9	1.4 ± 1.0	0.3 ± 0.1
phosphoenolpyruvate synthase	28 ± 5.1	25 ± 4.9	7.6 ± 2.0

(1 µmol substrate to product per minute)

Figure legends

Fig. 1. Stramenopile glycolytic C3 enzymes contain amino-terminal targeting signals. A. Comparison of *Blastocystis* amino-terminal sequences for TPI-GAPDH, PGK, PMG, and enolase with homologs from yeast showing the mitochondrial-like targeting signals. B. *Phaeodactylum tricornutum* glycolytic C3 enzyme amino-termini of TPI-GAPDH, PGK, PMG, enolase, and pyruvate kinase compared to yeast homologs demonstrate mitochondrial-like targeting signals.

Fig. 2. Stramenopile glycolytic enzyme amino-terminal mitochondrial-like targeting signals are sufficient to target GFP to mitochondria in the diatom *Phaeodactylum tricornutum*. A. The *Blastocystis* glycolytic enzymes TPI-GAPDH and PGK contain amino-terminal targeting signals that can target GFP to *P. tricornutum* mitochondria. B. Amino-terminal extensions on TPI-GAPDH, PGK, phosphoglycerate mutase (PGM), enolase and pyruvate kinase (PK) from the diatom *P. tricornutum* were cloned in front of GFP and constructs used to transform *P. tricornutum*. C. Amino terminal extensions on TPI-GAPDH and PGM from *Phytophthora infestans*, PK from *Achlya bisexualis* and TPI-GAPDH from *Saccharina latissima* were used as above to test for functionality of targeting information in *P. tricornutum.* DIC, Differential interference contrast microscopy. Chl, Chlorophyll *a* autofluorescence. GFP, Green fluorescent protein. Chl+GFP, Merged imaged showing the discrete (mitochondrial) localization of GFP. MitoTraker, MitoTraker Orange stain. MitoTraker+GFP, Merged image show considerable overlap of MitoTraker stain and GFP fluorescence. For the corresponding amino acid sequences used for GFP targeting, see Supplementary File 1. Scale bar 5 µm.

Fig. 3. The glycolytic enzymes TPI-GAPDH and PGK localize to mitochondria in the human parasite *Blastocystis.* Three-dimensional immunoconfocal microscopy reconstruction of optical sections (volume rendering) showing representative subcellular localization of PGK (blue) and TPI (red) in trophozoites (A-D, scale bar 3 µm). PGK (A) and TPI (B) volume signals show distinct distributions, consistent with localization within mitochondria, with considerable overlap. The merged image (C) provides a qualitative and the scatterplot (inset) of a quantitative measure of signal overlap. Co-localisation of MitoTracker (red) and PGK (green) and DAPI (blue) in trophozoites (E-I). Merged images MitoTracker/DAPI (E) PGK/DAPI (F) and MitoTracker/PGK (G) and all three markers together (H) show considerable overlap with the exception of the DAPI signals for the nuclei (asterisks). Scatterplots (inset) give a quantitative measure of signal overlap for each merged pair of markers (E-G, scale bar 2 µm).

Fig. 4. Stramenopile glycolytic enzymes contain mitochondrial-like amino-terminal targeting sequences. Representative stramenopiles with whole genome data known are shown. Presence of mitochondrial-like targeting signal is shown with a filled circle while open circle indicates no mitochondrial-like targeting signal. Where multiple isoforms with and without targeting signal exist, a half-filled circle is shown.

Fig. 5. *Phaeodactylum tricornutum* contains, similar to some other stramenopiles, multiple isoforms for the C3 part of glycolysis. The localization for all isoforms was tested via GFP-fusion constructs. A "pre" suffix means that the predicted targeting signal was used; if the suffix is missing the full length of the respective sequence was fused to GFP. The number is the JGI Protein ID and the result of each localization is mentioned. A star (*) marks images were a maximum intensity projection from a Z-Stack was used. Unclear indicates localization not possible to identify. TPI = Triosephosphate isomerase, GAPDH = Glyceraldehyde-3-phosphate dehydrogenase, PGK = Phosphoglycerate kinase, PGM = Phosphoglycerate mutase, ENO = Enolase, PK = Pyruvate kinase. DIC, Differential interference contrast microscopy. Chl, Chlorophyll *a* autofluorescence. GFP, Green fluorescent protein. Chl+GFP, Merged imaged showing the discrete localization of GFP compared to Chlorophyll autoflourescence. For the corresponding amino acid sequences used for GFP targeting, see Supplementary File 2. Scale bar 5 μm.

Fig. 6. Stramenopile glycolysis. Localization of glycolytic enzymes in the stramenopiles is distributed between cytosol and mitochondria based on our cell biological and biochemical data. For the intestinal parasite *Blastocystis*, the pay-off phase is solely localized to the mitochondrial matrix while for all other studied stramenopiles the pay-off phase is found in the cytosol as well as the mitochondrion. It is not known which intermediary glycolytic substrate is transported into mitochondria (indicated by question marks). Flow is shown in the direction of pyruvate only. TPI, triosephosphate isomeras; GAPDH, glyceraldehyde phosphate dehydrogenase; PGK, phosphoglycerate kinase; PGM, phosphoglycerate mutase.

A

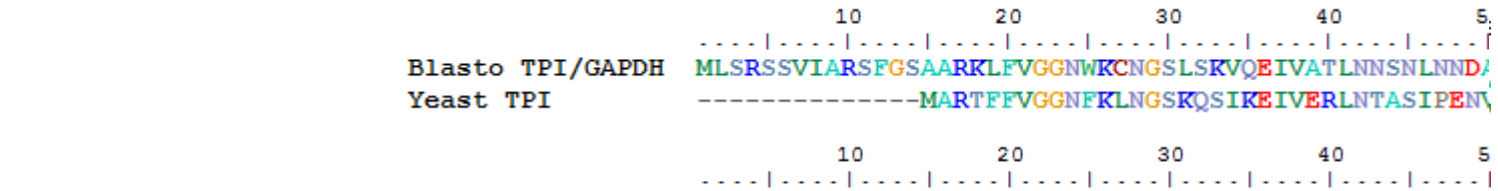
Blasto TPI/GAPDH
Yeast TPI
Blasto PGK
Yeast PGK
Blasto PGM
Yeast PGM
Blasto enolase
Yeast enolase

B

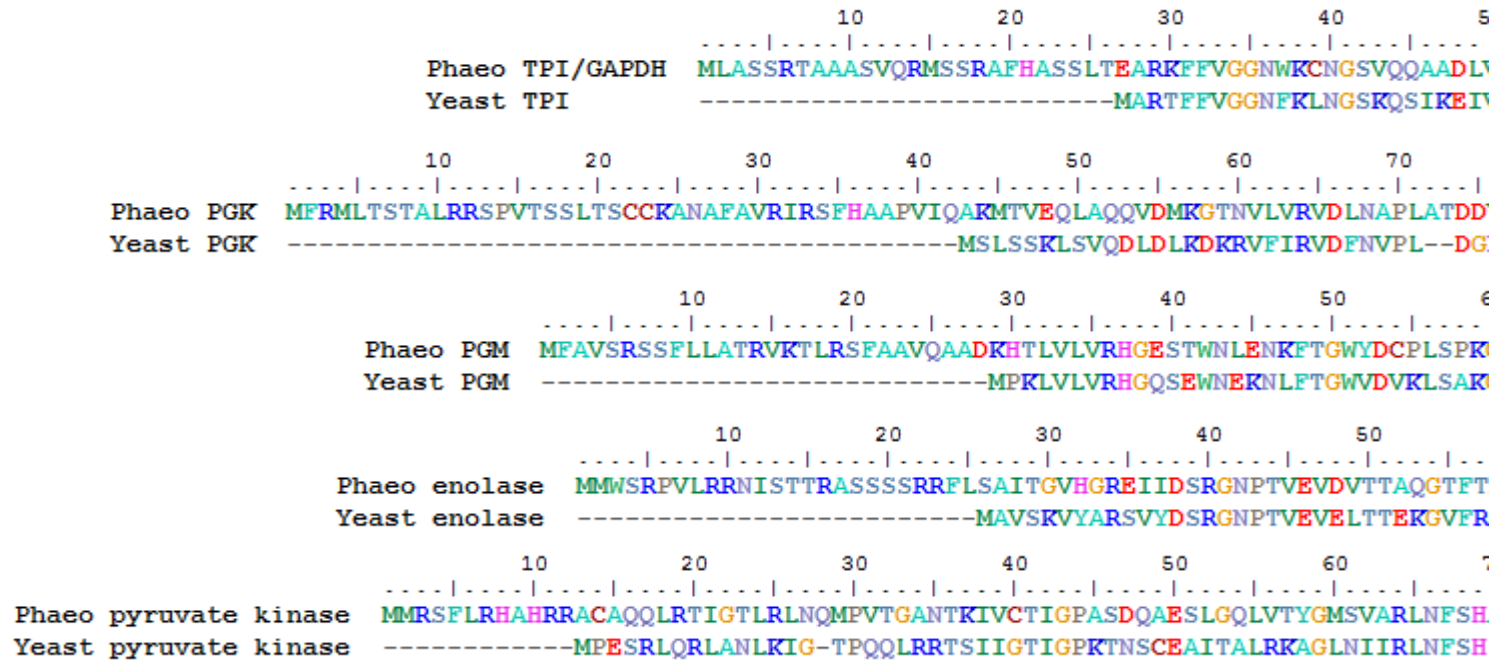
Phaeo TPI/GAPDH
Yeast TPI
Phaeo PGK
Yeast PGK
Phaeo PGM
Yeast PGM
Phaeo enolase
Yeast enolase
Phaeo pyruvate kinase
Yeast pyruvate kinase

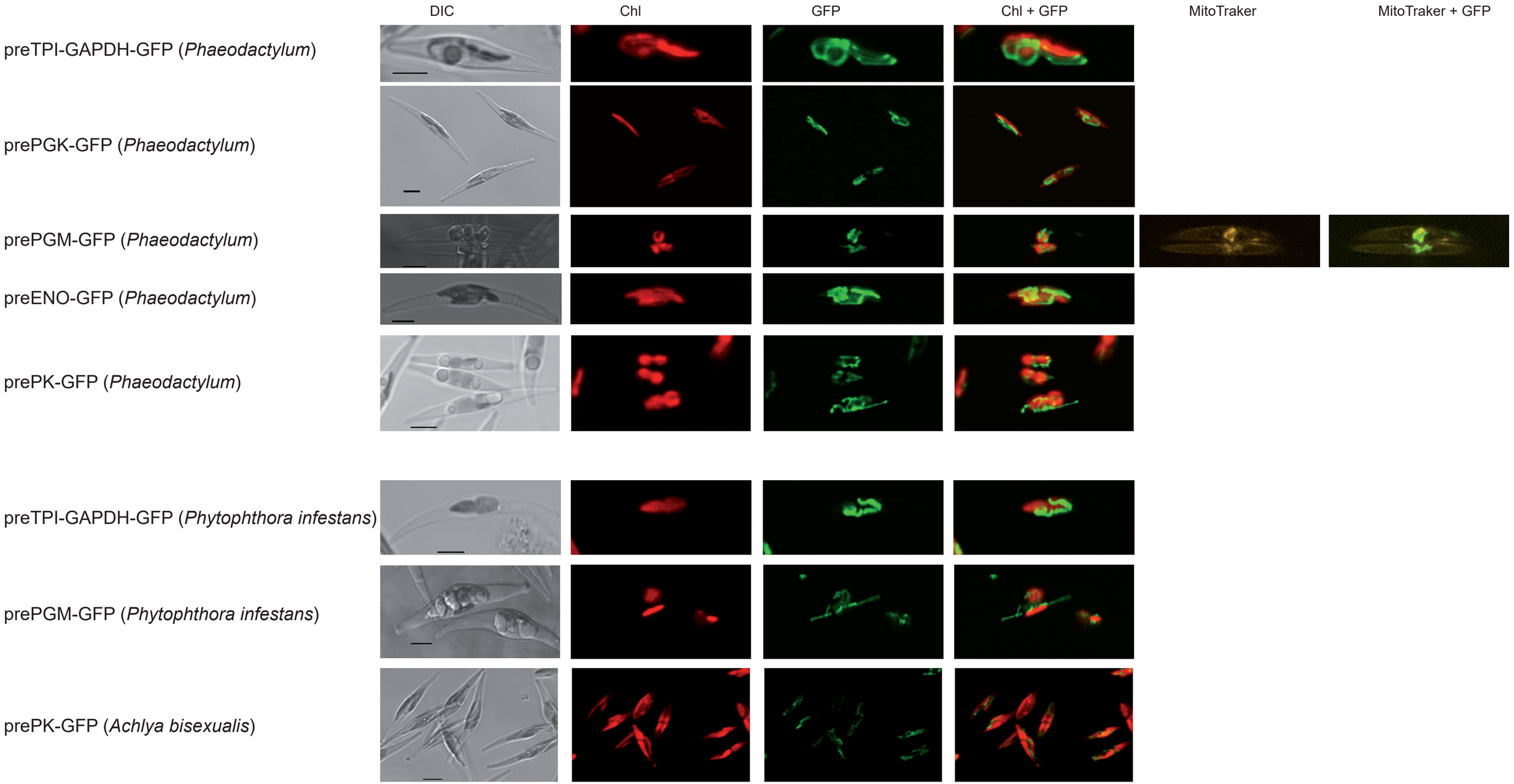
DIC
Chl
GFP
Chl + GFP
MitoTraker
MitoTraker + GFP
preTPI-GAPDH-GFP (*Phaeodactylum*)
prePGK-GFP (*Phaeodactylum*)
prePGM-GFP (*Phaeodactylum*)
preENO-GFP (*Phaeodactylum*)
prePK-GFP (*Phaeodactylum*)
preTPI-GAPDH-GFP (*Phytophthora infestans*)
prePGM-GFP (*Phytophthora infestans*)
prePK-GFP (*Achlya bisexualis*)

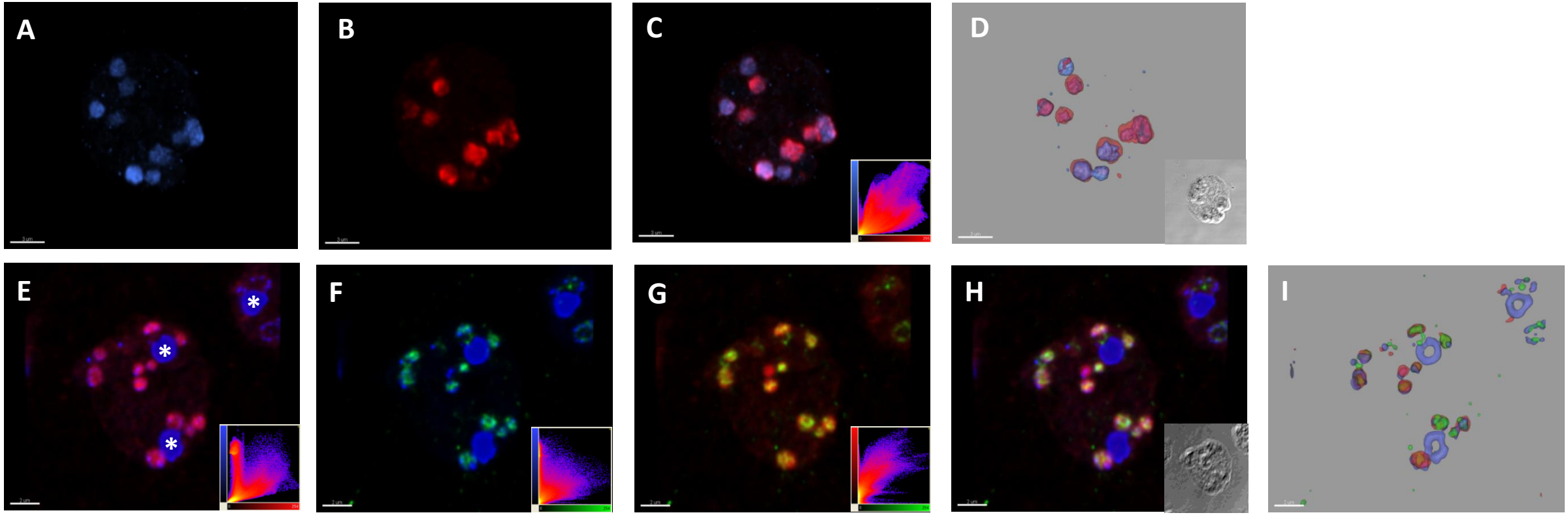
A
B
C
D
E
F
G
H
I

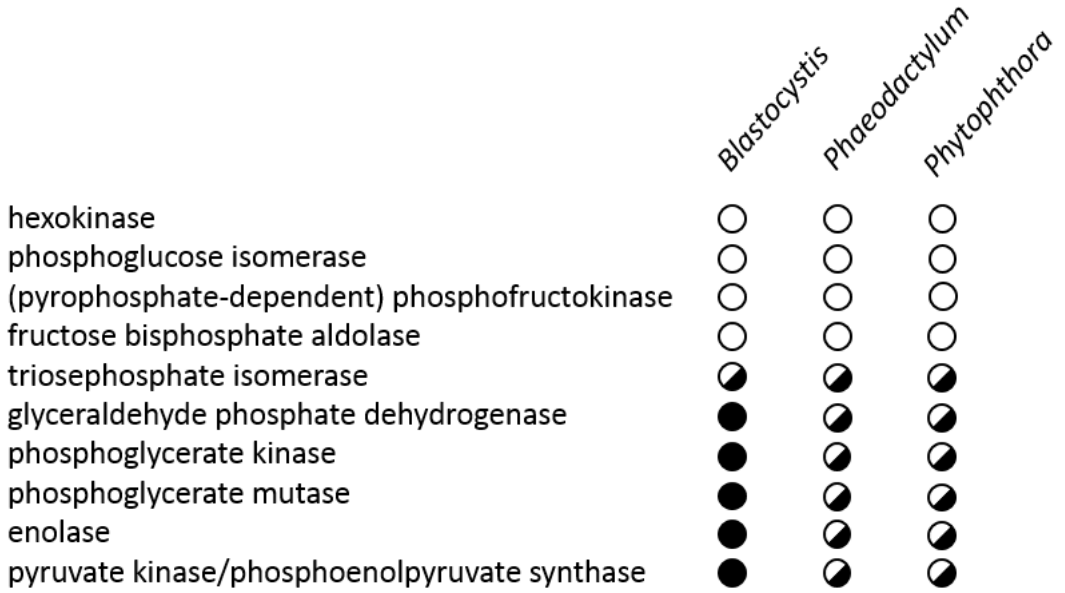
Blastocystis
Phaeodactylum
Phytophthora
hexokinase
phosphoglucose isomerase
(pyrophosphate-dependent) phosphofructokinase
fructose bisphosphate aldolase
triosephosphate isomerase
glyceraldehyde phosphate dehydrogenase
phosphoglycerate kinase
phosphoglycerate mutase
enolase
pyruvate kinase/phosphoenolpyruvate synthase

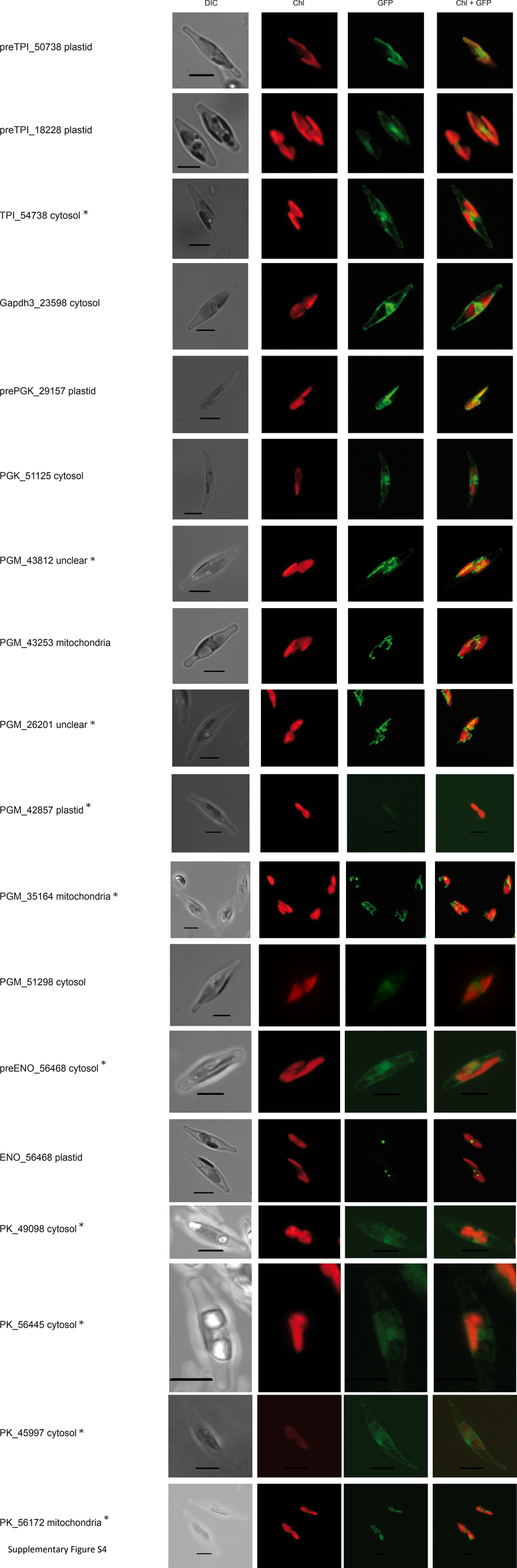

Supplementary Figure S4

stramenopile glycolysis

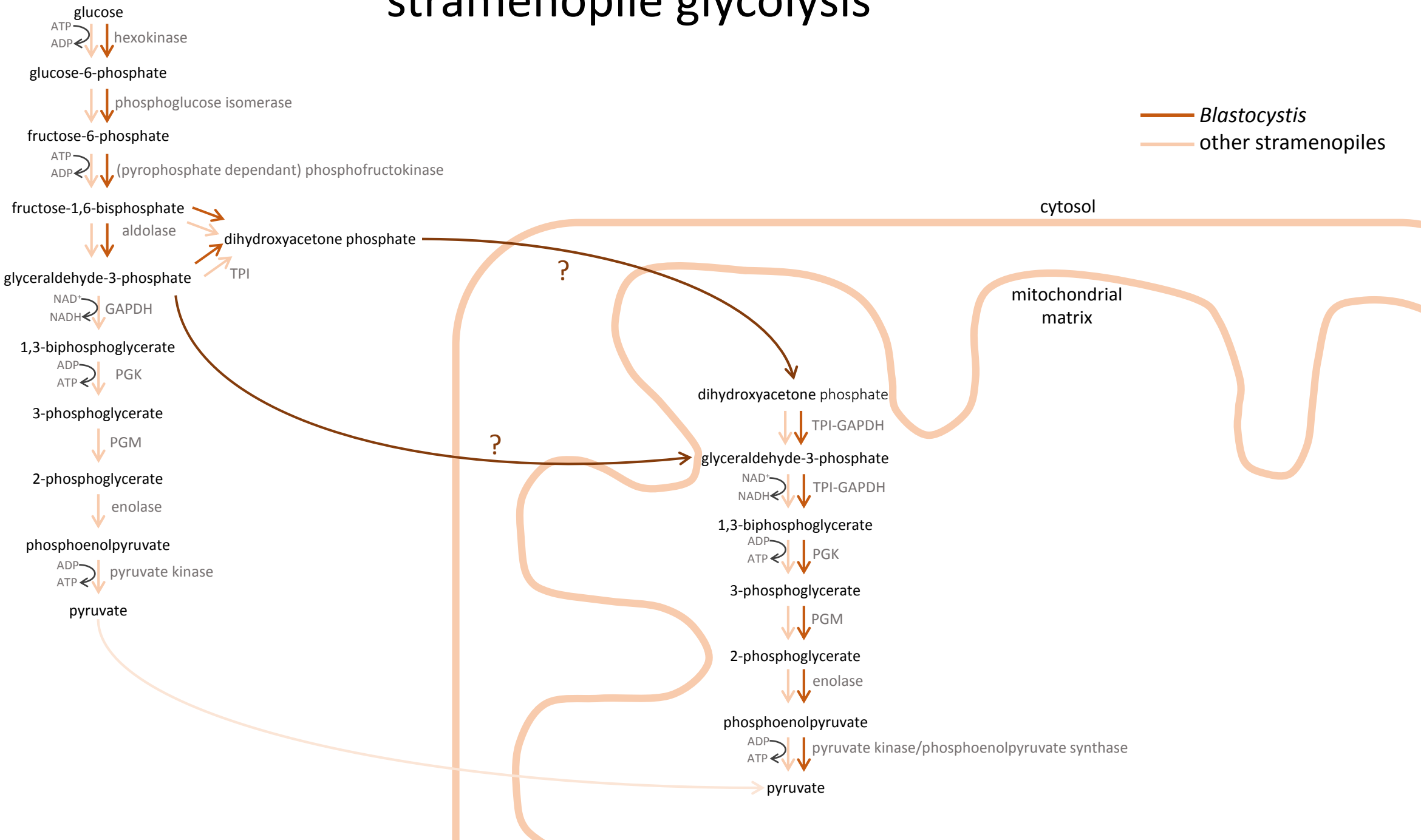

Supplementary figure legends

Figure S1. Phylogenetic analysis of glycolytic enzymes of the pay-off phase. A. Triosephosphate isomerase (TPI), 77 sequences and 167 amino acid positions were used to calculate the tree. Bacterial sequences were used as outgroup. B. Glyceraldehyde-3-phosphate dehydrogenase (GAPDH), only GAPDH from the C –type are illustrated in the tree. 96 sequences and 266 amino acid positions were used to calculate the tree. One branch caused long branch attraction (LBA) artifact and therefore is shortened in the figure. C. Phosphoglycerate kinase (PGK), 66 sequences and 360 amino acid positions were used to calculate the tree. D. Phosphoglycerate mutase (PGM), 96 sequences and 199 amino acid positions were used to calculate the tree. E. Enolase (ENO), 80 sequences and 345 amino acid positions were used to calculate the tree. F. Pyruvate kinase (PK), 80 sequences and 287 amino acid positions were used to calculate the tree. Values at nodes: posterior probabilities (P.P. >0.5) / rapid bootstrap values (BS>30%). Species name in bold = localization experimental proof (arrow = in this study, star Liaud *et. al* (2000)). TargetP analysis: M = mTP = mitochondria (bold indicates scores > 0.700), O = other, SP = signal peptide, C = cTP = chloroplast only for Viridiplantae, Rhodophyta and Glaucocystophyceae plant results was taken if non-plant results differ. N.D.: sequences not analyzed; not complete at N-terminus or start methionine is missing (proof by an alignment). Colour code: Viridiplantae, Stramenopiles, Alveolata, Rhizaria, Rhodophyta, Cryptophyta, Haptophyceae, Bacteria, other Eukaryota, Archaea, Cyanobacteria, Euglenozoa.

A. TPI

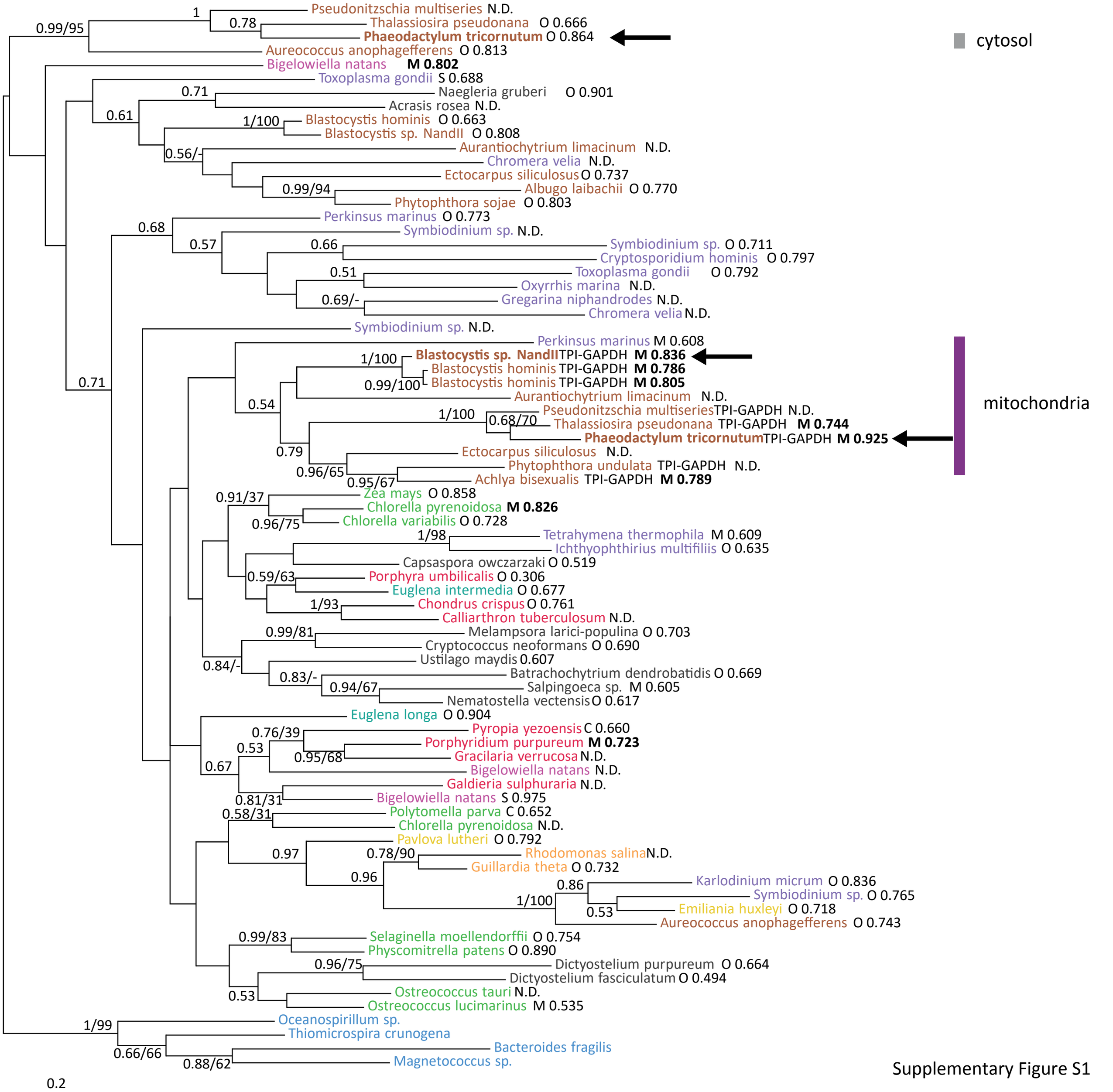

Supplementary Figure S1

B. GAPDH

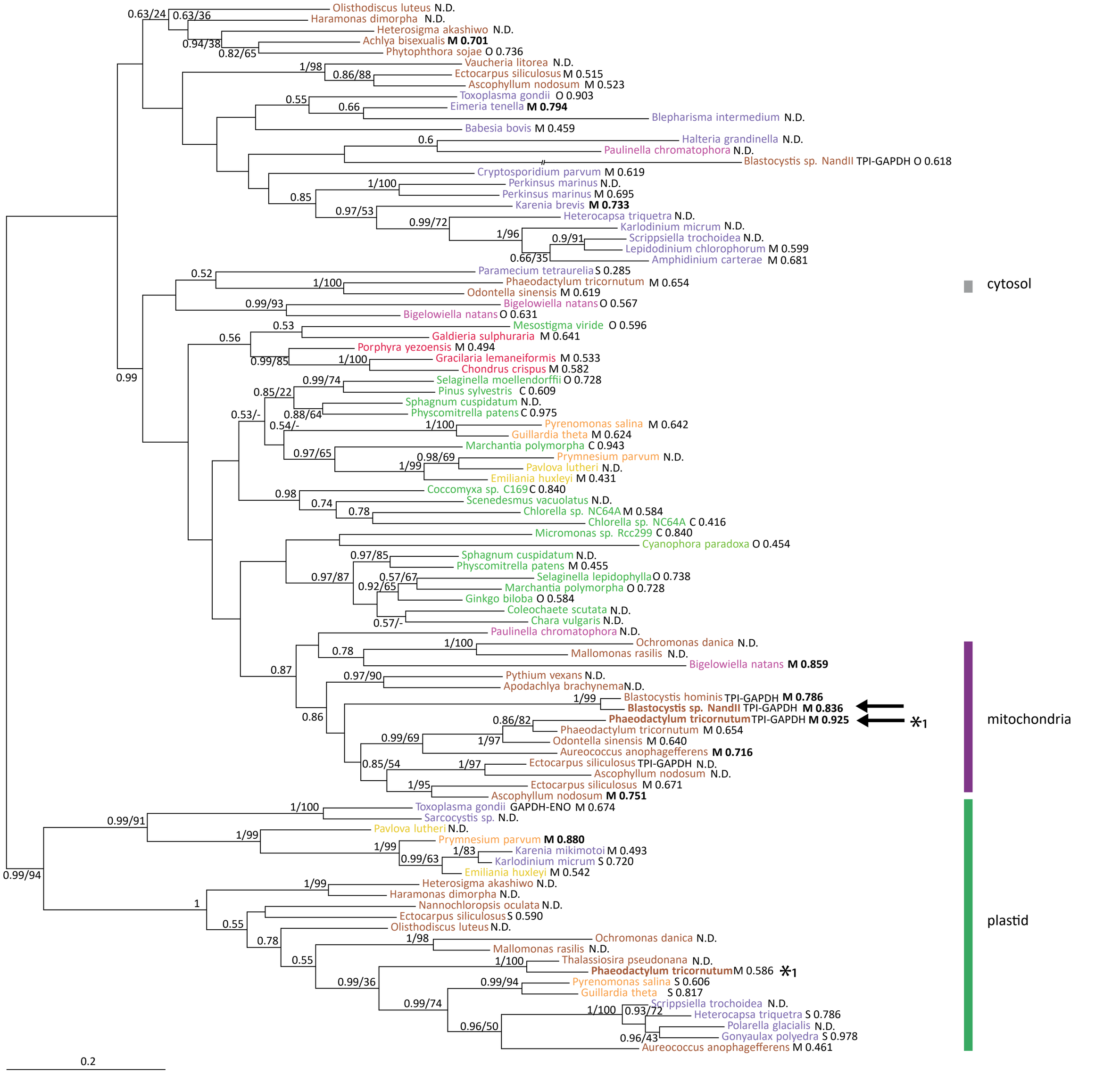

Supplementary Figure S1

C. PGK

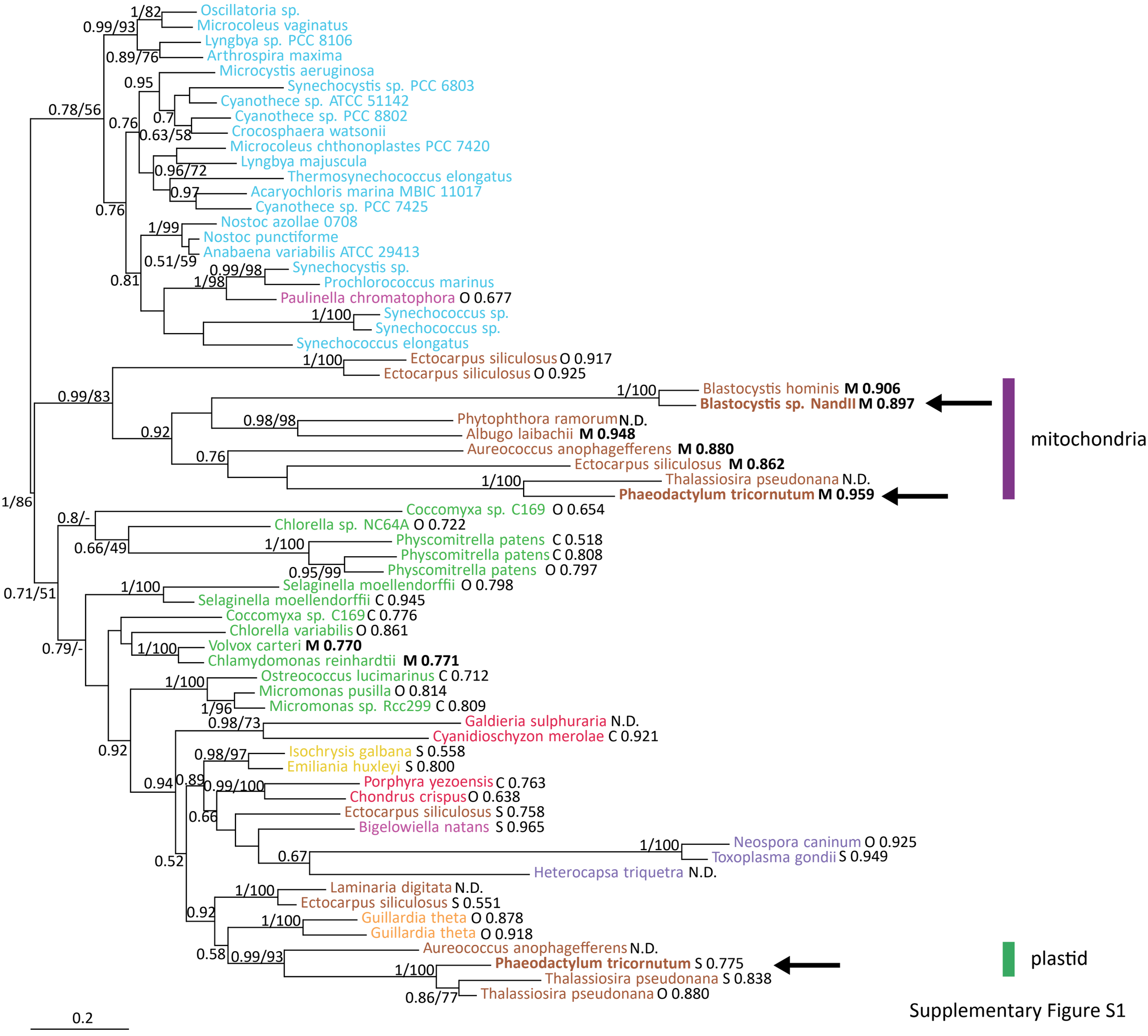

Supplementary Figure S1

D. PGM

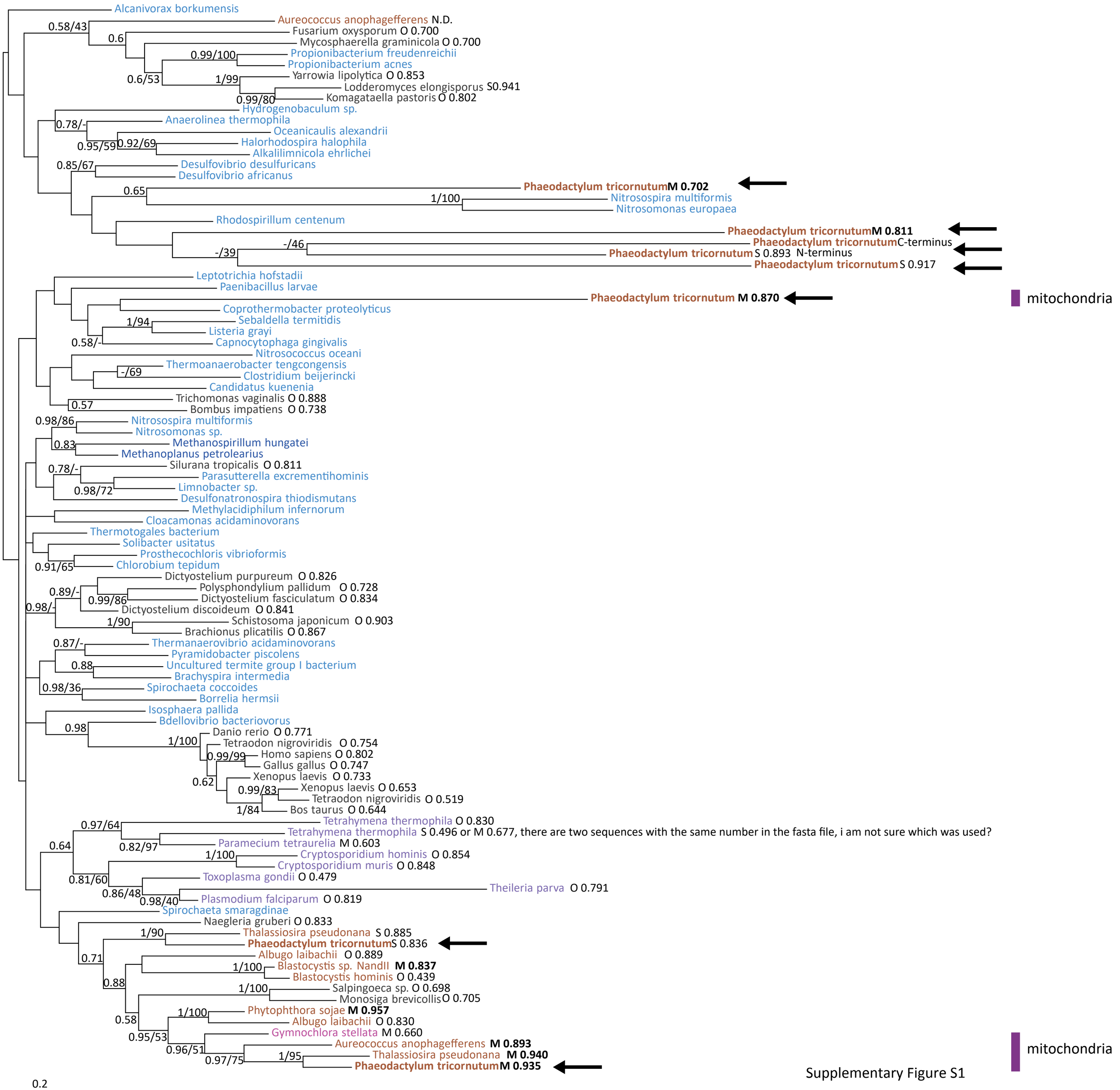

Supplementary Figure S1

E. ENO

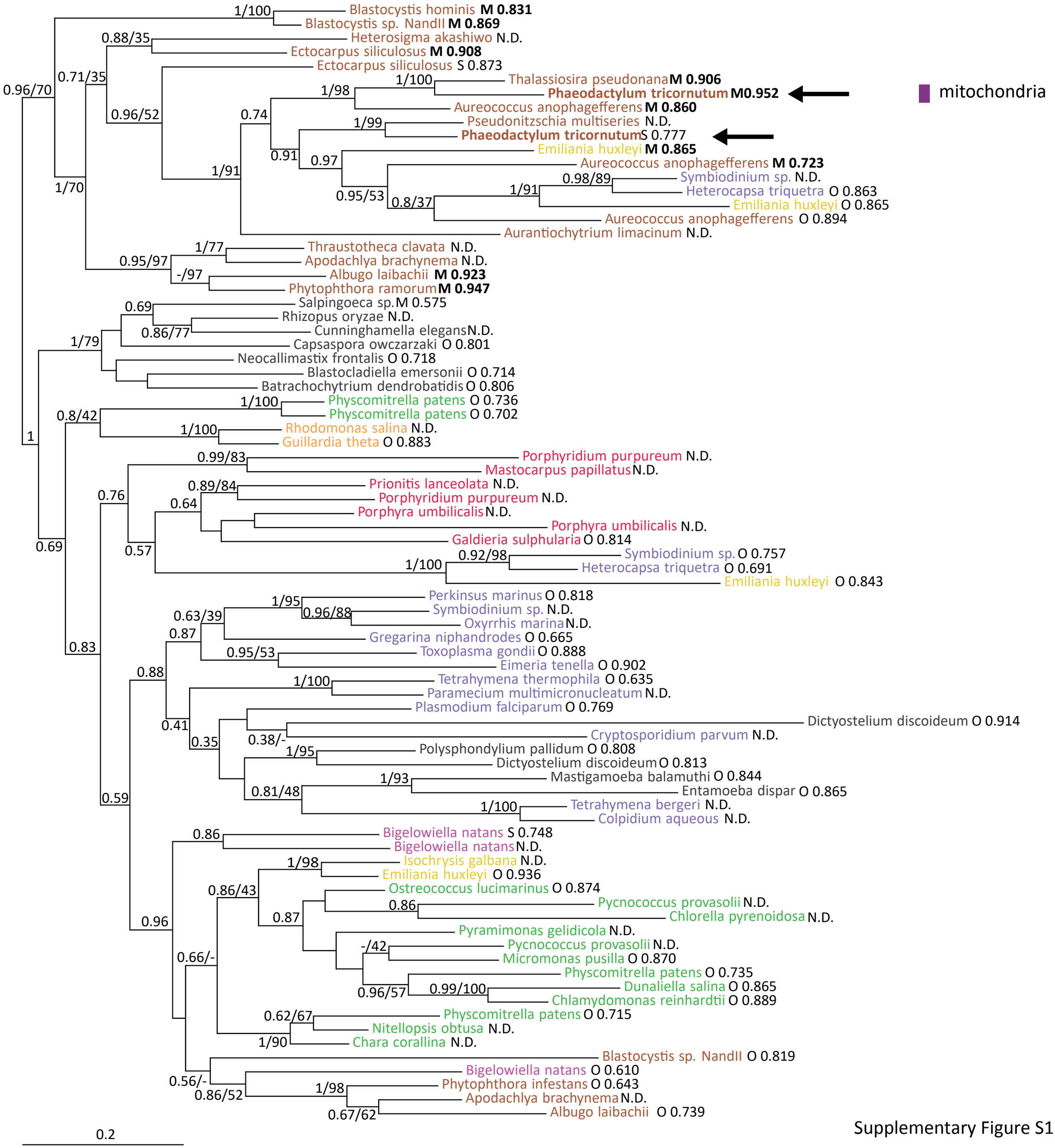

Supplementary Figure S1

F. PK

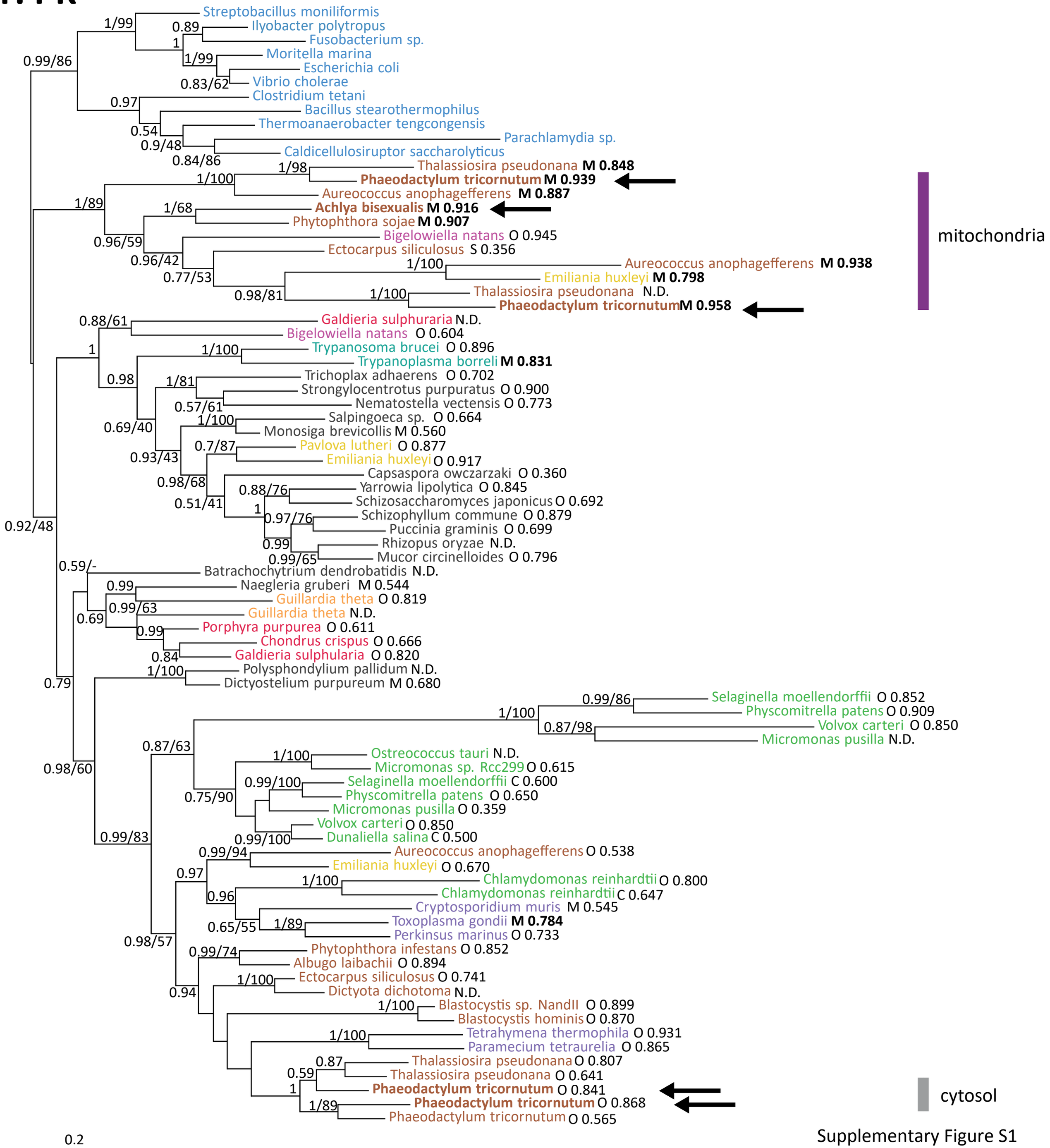

Supplementary Figure S1

Amino acid sequences of mitochondrial targeting sequences used in GFP targeting experiments as seen in Figure 2.

A.

> preTPI-GAPDH-GFP (*Blastocystis*) (OAO12326)

MLSRSSVIARSFGSAARKL

>prePGK-GFP (*Blastocystis*) (OAO15536)

MLSAFSKRLFSTGRTVN

B.

> preTPI-GAPDH-GFP (*Phaeodactylum*) (NCBI AF063804)

MLASSRTAAASVQRMSSRAFHASSLTEARKFFVGGNWKCNGS

>prePGK-GFP (*Phaeodactylum*)(JGI 48983)

MLFRMLTSTALRRSPVTTSLTCCCKANAFAVRIRSFHAAPVIQAKMTVEQLAQQ

>prePGM-GFP (*Phaeodactylum*)(JGI 33839)

MFAVSRSSFLLATRVKTLRSFAAVQAADKHTLVLLRHGESTWNLENKFTGWYDCP

>preENO-GFP (*Phaeodactylum*)(JGI 1572)

MMWSRPVLRRNISTTRASSSSRRFLSAITGVHGREIDSRGNPTVEVDVTTAQGT

>prePK-GFP (*Phaeodactylum*) (JGI 49002)

MMRSFLRHAQGRACAQHLRTIGTLRLNQMPVTGA

C.

>preTPI-GAPDH-GFP (*Phytophthora infestans*) (NCBI X64537)

MSFRQVFKTQARHMSSSSRKFFVGGNWKCNGSLGQAQELVGMLNTA

>prePGM-GFP (*Phytophthora infestans*) (PfGD Pi_011_55705_Feb05.seq)

MVLALRRPLAISSRVANRSLGMLRQQQKAMKHTHTLVLIRHGESEWNKKNLFTGWYDVQLSEKGNKEA

>prePK-GFP (*Achlya bisexualis*) (NCBI AAU81895)

MLARSLRSRAVRSFARGLSNKPSKNDAFSMT

>preTPI-GAPDH-GFP (*Saccharina latissima*) (NCBI ABU96661)

MFSAALSAAGAKAPSAARGFASSASRMSGRKFFVGGNWKCNGS

Phaeodactylum tricornutum **amino acid sequences used in GFP targeting experiments as seen in Figure 5.**

>preTPI_50738 plastid (pre-sequence) (JGI 50738) plastid

MTGDSTSLLDLISPDRERPQRKEPSRWIAFSVFPFVRFIPEAFATRLPYSIVMKFLALSVAALISSATAFAPTFR
GSPASTTASTTSLAARKPFISGNWKLN

>preTPI_18228 plastid (pre-sequence) (JGI 18228) plastid

MKFLALSVAALISSATAFAPTFRGSPASTTASTTSLAARKPFISGNWKLN

>TPI_54738 cytosol (242 Amino acids) (JGI 54738) cytosol

MPRPDGSSTPAAEGERKYLVAGNWKCNGTLASNEELVKTFNEAGPIPSNVEVAICCPSLYLPQLLSSLRDDIQIG
AQDCGVNDKNGAFTGEIGAFQIKDIGCDWVIIGHSERRDGFEMPGETPDLCAKKTRVAIDAGLKVMFCIGEKKEQ
REDGTTMDVCASQLEPLAAVLTESDWSSIAIAYEPVWAIGTGLTATPEMAQETHASIRDWISQNVSADVAGKVRI
QYGGSMKGANAKDLLEQ

>Gapdh3_23598 cytosol (full length) (JGI 23598) cytosol

MPVKCLVNGFGRIGRLCFRYAWDDPELEIVHVNDVCSCESAAYLVQYDSVHGTWSKSVVAAEDSQSFTVDGKLVT
FSQEKDFTKIDFASLGVDMVMECTGKFLTVKTLQPYFGMGVKQVVVSAPVKEDGALNVVLGCNHQKLTTDHTLVT
NASCTTNCLAPVVKVIQENFGIKHGCITTIHDVTGTQTLVDMPNTKKSDLRRARSGMTNLCPTSTGSATAIVEIY
PELKGKLNGLAVRVPLLNASLTDCVFEVNKEVTVEEVNAALKKASESGPLKGILGYETKPLVSTDYTNDTRSSII
DALSTQVIDKTMIKIYAWYDNEAGYSKRMAELCNIVAAMNITGQEPSFKYE

>prePGK_29157 plastid (pre-sequence) (JGI 29157) plastid

MKFVQAAIFALAASASTTAAFAPAKTFGVRSFAP

>PGK_51125 cytosol (193 Amino acids) (JGI 51125) cytosol

MASDMPKLAPGATRKRNVFDVIEALQKQSAKTILVRVDFNVPMNSDGKITDDSRIRGALPTIKAVVNAKCNAVLV
SHMGRPKLVQKAADDEETRQQRHELSLKPVADHLAKLLDQEVLFGDDCLHAQSTIRELPAEGGGVCLLENLRFYK
EEEKNGEDFRKTLASYADGYVNDAFGTSHRAHASVAGVPALLP

>PGM_43812 unclear (130 Amino acids) (JGI 43812) unclear localization, cytosol plus ER or mitochondria

MGRRTTHRRLFPALALIFAELIMSTAYSLAWRTSAACWTTTTGTACSRSRIATTRKVRRSRPNPCNPWHPVAFSF
FGTSSRRCRSSGSLYGEIDADAEGPDSPSADDRSVPTPSTTSSLSRSETLPPIPP

>PGM_43253 mitochondria (112 Amino acids) (JGI 43253) mitochondria

MASITLNRSRFTMITAIGMSHPRSHGTPRSVLLLLLRQFSSKDWNSKGTDSASRSGPVLIKKTPRSAAAAKLRST
APSLNGSTTDSTTGAVKHHPAHHYINGGTPCDPAPPP

>PGM_26201 unclear (408 Amino acids) (JGI 26201) unclear, mitochondria or ER

MLVPHPSGKAMRGLREEACRFLSSRSFGATLDATHARMGGNFVNSVQACNNGKRVCWHQRNRRTFSVVATQRNGI
GHRTTQGETEAVPRRHFTSLNQSTPFQLCFLRHGQSTWNRDNIFIGWTDTPLTDDGVLEARVAGKMLHKSGIRFD
EVHTSLLRRSIRTTNLALMELGQEYLPVHKHWRLNERCYGDLVGKNKKEVVMQHGADQVKRWRRSYDEPPPPMSD
DHPYHPARDPRYQNILDELPKSESLKNTVERSSLYWDEVLAPALREGKTLLVVGHENNLRSLLMRLEDIAPEDII
NLSLPRAVPLAYRLDENLKPLPREDGKLDEATGFLKGTWLGGDQAVSEILDRDHKQVYDTAITTNLEIGQDREKW
NNWMEFIMGKPSAKQKRIGGDKQNGFAGGAAIP

>PGM_42857 plastid (175 Amino acids) (JGI 42857) plastid

MAMDAITMRKLTLTMAVLLIVSGCEALLVFLPRRSPFTVISTRSSTNSAGLLHLHSKANESDGLEGKWIKVSSAL
DEGVDAANEEKEGAFLSSDYNSMNGYNTDLNRYHTMLRERGTFVEALFGQRRSFVIAKRDGDENEDGWRDMRRQR
RPLWKHLLRLPISVAKNVLWKPPQP

>PGM_35164 mitochondria (351 Amino acids) (JGI 35164) mitochondria

MRIPCRRLHPQLSAKGTRRPFQYSSSNSIDDQHRSSHLDASPGRHIVVRHGQSVWNKGSNQLERFTGWTNVGLSE
NGQRQAVQAARKLHGYSIDCAYVSLLQRSQATLRLMLEELNDQGRRSEGYDDLTTDIPVISSWRLNERHYGALTG
QSKLQAEQLFGKAQLDLWRYSYKIPPPPMDPDTFSSWKHQAHCQMATYIHHRHNRSRVIEKGNSVWDSSRAVMPR
SEAFFDVLQRIVPLWKYGIAPRLARGETVLLVGHANSVKALLCLLDPHTVTPTSIGALKIPNTTPLVYQLIRDYP
GASTSVPASFPVLGDLRVVIPPSNSTRYPLSGTWLEDPPVARDAGTAVEEP

>PGM_51298 cytosol (131 Amino acids) (JGI 51298) cytosol. If a shorter version, starting from the second Methionine is used, a localization at the plastid as a blob like structure is the result (data not shown).

MCDESRQTATPMIHFEIFRFSDPLVRQDRQAPHLSLTSTVKILSDSNLHKLFIMMLRSLVLALSWTVASAFTHQS
TFWGRTAVTNSRILSLSPPTDASSSALCMKYMLVLVRHGESTWNKENRFTGWVDCP

>preENO_56468 cytosol (66 Amino acids) (JGI56468) cytosol. Start Methionine from GFP was not included in the construct.

MLFKPSTLLALFAVAGTTLAFAPRSTTTPLTSTTRGSASSSVTTLAMSGITGVLAREILDSRGNPV

>ENO_56468 plastid (443 Amino acids) (JGI56468) plastid

MLFKPSTLLALFAVAGTTLAFAPRSTTTPLTSTTRGSASSSVTTLAMSGITGVLAREILDSRGNPTVEVEVTTAD
GVFRASVPSGASTDAYEAVELRDGGDRYMGKGVLQAVQNVNDILGPAVMGMDPVGQGSVDDVMLELDGTPNKANL
GANAILGVSLAVAKAGAAAKKVPLYRHFADLAGNNLDTYTMPVPCFNVINGGSHAGNKLAFQEYFVIPTGAKSFA
EAMQIGCEVYHTLGKIIKAKFGGDATLIGDEGGFAPPCDNREGCELIMEAISKAGYDGKCKIGLDVAASEFKVKG
KDEYDLDFKYDGDIVSGEELGNLYQSLAADFPIVTIEDPFDEDDWENWSKFTTKNGATFQVVGDDLTVTNIEKIE
RAIDEKACTCLLLKVNQIGSISESIAAVTKAKKAGWGVMTSHRSGETEDTYIADLAVGLCTGQIKTGA

>PK_49098 cytosol (507 Amino acids) (JGI: 49098) cytosol

MTASQTKITASGPELRGANITLDTIMKKTDVSTRQTKIVCTLGPACWEVEQLESLIDAGLSIARFNFSHGDHEGH
KACLDRLRQAADHKKKHVAVMLDTKGPEIRSGFFADGAKKISLVKGETIVLTSDYSFKGDKHKLACSYPVLAKSV
TPGQQILVADGSLVLTVLSCDEAAGEVSCRIENNAGIGERKNMNLPGVIVDLPTLTDKDIDDIQNWGIVNDIDFI
AASFVRKASDVHKIREVLGEKGKGIKIICKIENQEGMDNYDEILEATDAIMVARGDLGMEIPPEKVFLAQKMMIR

QANIAGKPVVTATQMLESMITNPRPTRAECSDVANAVLDGTDCVMLSGETANGEYPTAAVTIMSETCCEAEGAQN
TNMLYQAVRNSTLSQYGILSTSESIASSAAKTAIDVGAKAIIVCSESGMTATQVAKFRPGRPIHVLTHDVRVARQ
CSGYLRGASVEVISSMDQMDPAIDAYIERCKANGKAVAGDAFVVVTGTVAQRGVTNA

>PK_56445 cytosol (538 Amino acids) (JGI 56445) cytosol

MSLSQSSDVPILAGGFITLDTVKHPTNTINRRTKIVCTIGPACWNVDQLEILIESGMNVARFNFSHGDHAGHGAV
LERVRQAAQNKGRNIAILLDTKGPEIRTGFFANGASKIELVKGETIVLTSDYKFKGDQHKLACSYPALAQSVTQG
QQILVADGSLVLTVLQTDEAAGEVSCRIDNNASMGERKNMNLPGVKVDLPTFTEKDVDDIVNFGIKHKVDFIAAS
FVRKQSDVANLRQLLAENGGQQIKICCKIENQEGLENYDEILQATDSIMVARGDLGMEIPPAKVFLAQKMMIREA
NIAGKPVITATQMLESMINNPRPTRAECSDVANAVLDGTDCVMLSGETANGPYFEEAVKVMARTCCEAENSRNYN
SLYSAVRSSVMAKYGSVPPEESLASSAVKTAIDVNARLILVLSESGMTAGYVSKFRPERAIVCLTPSDAVARQTG
GILKGVHSYVVDNLDNTEELIAETGVEAVKAGIASVGDLMVVVSGTLYGIGKNNQVRVSVIEAPEGTVKETPAAM
KRLVSFVYAADEI

>PK_45997 cytosol (533 Amino acids) (JGI 45997) cytosol

MLSSTSTIPKLDGEVVTLSIIKKPTETKKRRTKIICTLGPACWSEEGLGQLMDAGMNVARFNFSHGDHEGHGKVL
ERLRKVAKEKKRNIAVLLDTKGPEIRTGFFADGIDKINLSKGDTIVLTTDYDFKGDSKRLACSYPTLAKSVTQGQ
AILIADGSLVLTVLSIDTANNEVQCRVENNASIGERKNMNLPGVVVDLPTFTERDVNDIVNFGIKSKVDFIAASF
VRKGSDVTNLRKLLADNGGPQIKIICKIENQEGLENYGDILEHTDAIMVARGDLGMEIPSSKVFLAQKYMIREAN
VAGKPVVTATQMLESMVTNPRPTRAECSDVANAVYDGTDAVMLSGETANGPHFEKAVLVMARTCCEAESSRNYNL
LFQSVRNSIVIARGGLSTGESMASSAVKSALDIEAKLIVVMSETGKMGNYVAKFRPGLSVLCMTPNETAARQASG
LLLGMHTVVVDSLEKSEELVEELNYELVQSNFLKPGDKMVVIAGRMAGMKEQLRIVTLDEGKSYGHIVSGTSFFF
ERTRLLDF

>PK_56172 mitochondria (86 Amino acids) (JGI: 56172) mitochondria

MFRRAVLSLSTRAIRTPVPCSVARGDASQVRSLAQTTFYLPDPADRSQDVHNRGNLQLSKIVATIGPTSEQEEPL
RLVTDAGMRIM